Effect of Di and Trivalent Substitution in B site of Sodium vanadium phosphate on Cyclability

By

JAYA DHARANI P V

(Reg No. 21PPH003)

Supervisor

Dr. B. Nalini

Department of Physics

A Thesis submitted to

AVINASHILINGAM INSTITUTE FOR HOME SCIENCE AND HIGHER EDUCATION FOR WOMEN, COIMBATORE – 641 043.

In Partial Fulfilment of the requirements for the award of Degree

MASTER OF SCIENCE IN PHYSICS

MAY 2023

Effect of Di and Trivalent Substitution in B site of Sodium vanadium phosphate on Cyclability

By

JAYA DHARANI P V

(Reg No. 21PPH003)

Supervisor

Dr. B. Nalini

Department of Physics

A Thesis submitted to

AVINASHILINGAM INSTITUTE FOR HOME SCIENCE AND HIGHER EDUCATION FOR WOMEN, COIMBATORE – 641 043.

In Partial Fulfilment of the requirements for the award of Degree

MASTER OF SCIENCE IN PHYSICS

MAY 2023

CERTIFIED AS A BONAFIDE RESEARCH WORK

12/05/23

Signature of the Head of the Department

Dr. J. SHANTHI, M.Sc., M.Phil., Ph.D.,
Professor and Head
Department of Physics
Avinashilingam Institute for Home Science
and Higher Education For Women
Coimbatore - 641 043.

12/05/2023

Signature of the Supervisor

ACKNOWLEDGEMENT

ACKNOWLEDGEMENT

We owe our sincere thanks to lord almighty, our reverent **founder Dr. T.S. Avinashilingam Ayya** and our **Amma Dr. Rajammal P. Devadas** and my lovable parents. Without whom we should have been nothing, for showering their generous blessing upon us in all endeavors.

I owe my sincere thanks to **lord almighty** and **my lovable parents** for showering their generous blessings upon me in all endeavours.

I wish to express my gratitude to **Prof. S.P. Thyagarajan** Ph.D, M.D., D.S, FAMS, FNASc, FIMSA,FABMS, FFTM (Glasgow, UK), Chancellor, Avinashilingam Institute for Home Science and higher education for women, Coimbatore, for providing the facilities to conduct this study.

I extend my thanks to **Dr. V. Bharathi Harishankar** Ph.D., FRSA, Vice Chancellor, Avinashilingam Institute for Home Science and higher education for women, Coimbatore, for providing flamboyant help towards the completion of the study.

I record my deep sense of gratitude and indebtedness to **Dr.(Mrs) S. Kowsalya** M.Sc., M.Phil, Ph.D, Registrar, Avinashilingam Institute for Home Science and higher education for women, Coimbatore, for providing adequate help for the study.

I gratefully record my sincere thanks to **Dr.(Mrs.) G. Padmavathi** M.Sc., M.Phil., Ph.D., Dean, School of Physical Sciences and Computational Sciences, Avinashilingam Institute for Home Science and Higher Education for Women, Coimbatore, for timely help rendered throughout the course of this work

I whole heartily thank **Dr.(Mrs.) J. Shanthi,** M.Sc., M.Phil., Ph.D., Professor and Head, Department of Physics, Avinashilingam Institute for Home Science and Higher Education for Women, Coimbatore, for her encouragement and generous help which was of great value.

I express my heartiest thanks to my guide **Dr. (Mrs.) B. Nalini,** M.Sc., Ph.D., M.S (Edu.Mgt.), STA fellow, AIST Fellow (Japan), Assistant Professor, Avinashilingam Institute for Home Science and Higher Education for Women, University, Coimbatore, for her valuable guidance learned counsel, cordial treatment, keen interest, constant encouragement and care rendered throughout the course of my investigation.

I sincerely thank all **the staff members** of the Department of Physics, Avinashilingam Institute for Home Science and higher education for women, Coimbatore, for their help and support.

I would like to express my special thanks to **my parents, my friends** and all **my well-wishers** for their constant encouragement, support and help in carrying out this work successfully.

JAYA DHARANI P V

CONTENT

CONTENT

LIST OF FIGURES

LIST OF TABLES

INTRODUCTION

CHAPTER I

INTRODUCTION

1.1. Batteries

A battery is an electrochemical device that converts chemical energy directly into electrical energy by means of an electrochemical oxidation-reduction (redox) reaction. Every battery (cell) has a cathode (positive plate) and an anode (negative plate). These electrodes must be separated by and are immersed in an electrolyte that permits the passage of ions between the electrodes. **[1]**

The anode is a negative electrode that produces electrons to the external circuit to which the battery is connected. When batteries are connected, an electron build-up is initiated at the anode which causes a potential difference between the two electrodes.

The electrons naturally then try to redistribute themselves, this is prevented by the electrolyte, so when an electrical circuit is connected, it provides a clear path for the electrons to move from the anode to the cathode thereby powering the circuit to which it is connected.

By changing the arrangement and material used to build the anode, cathode and electrolyte can be achieve many different types of battery chemistries enabling us to design different types of battery cells. **[2]**

1.1.1. Working principle

A battery works on the principle of oxidation and reduction reaction of an electrolyte with metals. When two dissimilar metallic substances, called electrode, are placed in a dilute electrolyte, oxidation and reduction reaction takes place in the electrodes depending upon the electron affinity of the metal of the electrodes.

A schematic representation of working of battery is shown in Figure 1.1.

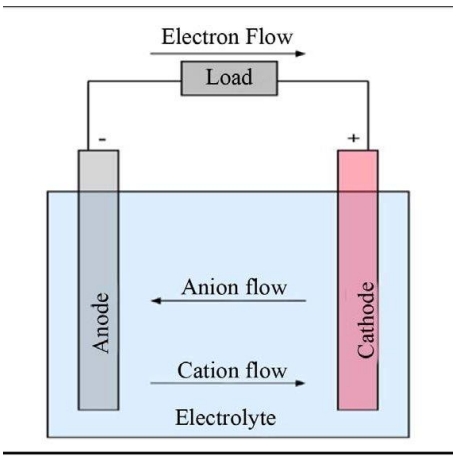

Figure 1.1. Schematic representation of working of a battery

1.1.2. Types of batteries

Batteries can be classified into different categories and types, ranging from chemical composition, size, form factor and use causes.

There are two types of batteries.

- Primary batteries
- Secondary batteries.

1.1.2.1. Primary batteries

Primary batteries (Figure 1.2.) are batteries that cannot be recharged once depleted. Primary batteries are made of electrochemical cells whose electrochemical reaction cannot be reversed.

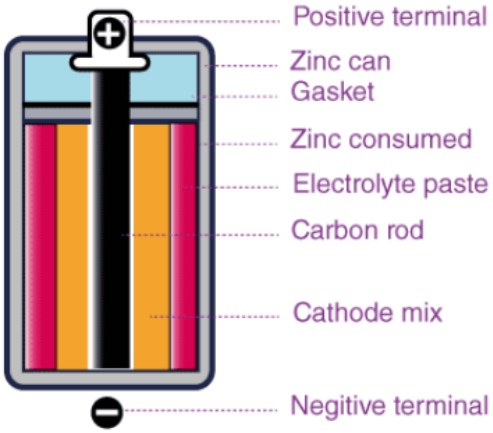

Figure 1.2. Primary Battery

Primary batteries are commonly used in standalone applications where charging is impractical or impossible. A good example of which is in military grade devices and battery powered equipment. It will be impractical to use rechargeable batteries as recharging a battery will be the last thing in the mind of the soldiers. Primary batteries always have high specific energy and the systems in which they are used are always designed to consume low amount of power to enable the battery last as long as possible.

Some common primary batteries

- Alkaline batteries
- Button cell battery

1.1.2.2. Secondary batteries

Secondary batteries are batteries with electrochemical cells whose chemical reactions can be reversed by applying a certain voltage to the battery in the reversed direction. (Figure 1.3.)

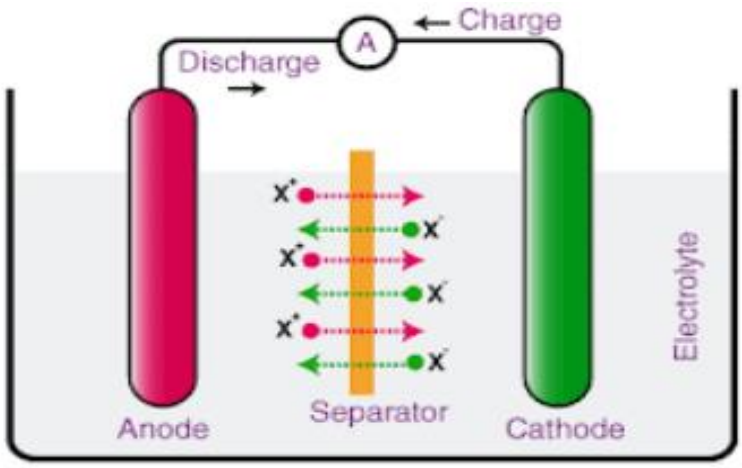

Figure 1.3. Secondary Battery

Small capacity secondary batteries are used to power portable electronic devices like mobile phones, and other gadgets and appliances while heavy-duty batteries are used in powering diverse electric vehicles and other high drain applications like load levelling in electricity generation. They are also used as standalone power sources alongside Inverters to supply electricity.

Some of the secondary batteries

- Lithium-ion batteries
- Sodium-ion batteries
- Lead acid batteries
- Nickel Cadmium batteries

1.2. Lithium-ion batteries

A lithium-ion (Li-ion) battery is an advanced battery technology that uses lithium ions as a key component of its electrochemistry. During a discharge cycle, lithium atoms in the anode are ionized and separated from their electrons. The lithium ions move from the anode and pass through the electrolyte until they reach the cathode, where they recombine with their electrons and electrically neutralize. The lithium ions are small enough to be able to move through a micro-permeable separator between the anode and cathode. In part because of lithium's small size (third only to hydrogen and helium), Li-ion batteries are capable of having a very high voltage and charge storage per unit mass and unit volume. A schematic illustration of Lithium-ion battery is shown in Figure 1.4.

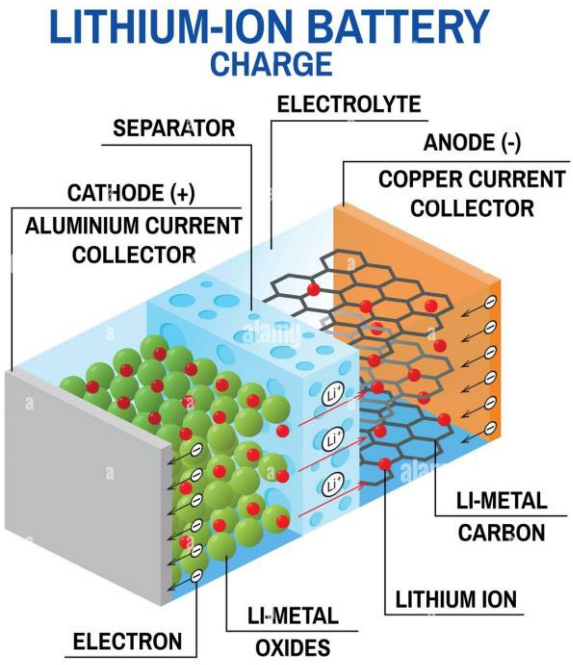

Figure 1.4. Schematic illustration of lithium-ion battery

Li-ion batteries (Figure 1.5.**)** can use a number of different materials as electrodes. The most common combination is that of lithium cobalt oxide (cathode) and graphite (anode), which is most commonly found in portable electronic devices such as cell phones and laptops. Other cathode materials include lithium manganese oxide (used in hybrid electric and electric automobiles) and lithium iron phosphate. Li-ion batteries typically use ether (a class of organic compounds) as an electrolyte. **[3]**

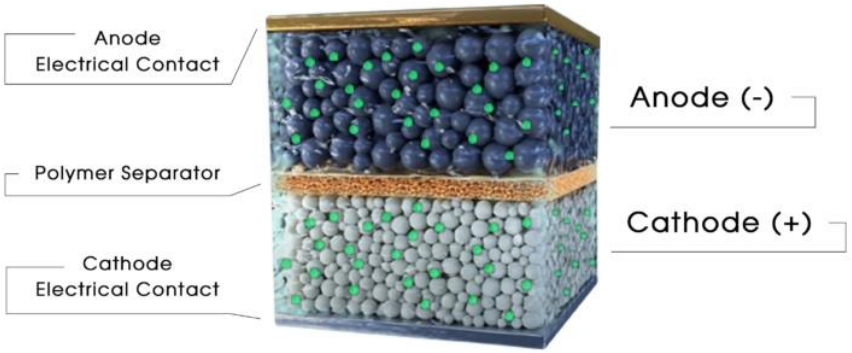

Figure 1.5. Structure of lithium-ion battery

1.2.1. Disadvantages of Lithium-ion batteries

- **Expensive** - The production of Lithium-ion batteries can be a rather expensive affair. The overall production cost of these batteries is around 40% higher than nickel-metal hydride batteries.
- **Protection required** - Lithium-ion cells and batteries are not as robust as some other rechargeable technologies, they require protection from being over charged and discharged.
- **Aging effect** - Lithium-ion battery will naturally degrade as they suffer from ageing. Normally Lithium-ion batteries will only be able to with stand 500 - 1000 charge and discharge cycles before their capacity falls to 50%.
- **Transportation problems** - This Lithium-ion battery disadvantage has come to the fore in recent years. A lot of restrictions are in place for the transportation of Lithium-ion batteries especially large quantities by air.
- **Deep discharge** - Lithium-ion battery has low self-discharge. The general integrity of this battery remains intact even if partially discharged. However, deep discharge or when the voltage of a Lithium-ion cell drops below a certain level, it becomes unusable.

1.2.2. Alternatives to lithium-ion batteries

Lithium-ion batteries currently dominate energy storage technology because of their capacity, rechargeability and price make them ideal for both consumer and industrial applications.

However, the advent of renewable energy equipment, electric vehicles, and the issues surrounding lithium extraction and safety are forcing markets to find batteries independent of the alkali metal. As a result of this demand, numerous lithium battery alternatives are in development that could shift the power balance for energy storage — given they are feasible, and more importantly, scalable. **[4]**

Three potential alternatives to lithium-ion batteries [5]

- Solid state batteries
- Lithium sulphur
- Sodium ion batteries
- **Solid state batteries**

Figure 1.6. Schematic diagram of solid-state battery

A solid-state battery has the same components as that of a lithium-ion battery but it uses a solid electrolyte and not liquid. The solid electrolyte in a solid-state battery plays the role of a separator as well.

Currently, solid-state batteries are used in devices like:

- Pacemakers
- Smart watches

But the current and on-going research on solid-state lithium metal batteries aims to be a game changer for the electric vehicle technology and speed up the shift away from fossil fuel-powered vehicles. Lower cost could make a big difference, given that at 30 per cent of the total cost, battery expenses are a key driver of the vehicle (EV) costs.

The development of solid-state batteries that can be manufactured at a large scale is one of the most important challenges in the industry today. The ambition is to develop solid-state batteries, suitable for use in electric vehicles, which substantially surpass the performance, safety and processing limitations of lithium-ion batteries. In contrast to research into lithium-ion batteries, which will provide incremental gains in performance towards theoretical limits, research into solid-state batteries is long term and high risk but also has the potential to bring high rewards.

- **Lithium-Sulphur battery**

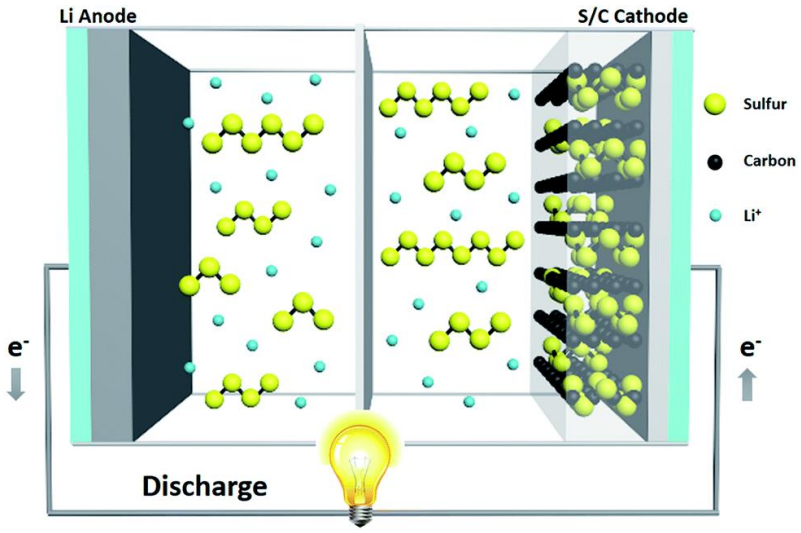

Figure 1.7. Diagrammatic representation of Lithium-Sulphur battery

The lithium–sulfur battery (Li–S battery) is a type of rechargeable battery. It is notable for its high specific energy. The low atomic weight of lithium and moderate atomic weight of sulfur means that Li–S batteries are relatively light (about the density of water). **[6]**

Lithium–sulfur batteries may displace lithium-ion cells because of their higher energy density and reduced cost. This is due to the use of sulfur instead of cobalt, a common element in lithium-ion batteries.[4] Li–S batteries offer specific energies on the order of 550 Wh/kg,[1] while lithium-ion batteries are in the range of 150–260 Wh/kg.

- **Sodium-ion batteries**

Figure 1.8. Sodium-ion battery

A sodium ion battery is a powerhouse of performance that optimizes a sodium ion cell for the electric output. Sodium-ion batteries are an emerging technology with promising cost, safety, sustainability and performance advantages over commercialized lithium-ion batteries. Key advantages include the use of widely available and inexpensive raw materials and a rapidly scalable technology based around existing lithium-ion production methods. These properties make sodium-ion batteries especially important in global demand for carbon-neutral energy-storage solutions. **[7]**

Out of these potential alternatives, sodium ion batteries are discussed below.

1.3. Sodium ion batteries

A sodium-ion battery is a type of rechargeable battery comparable to the ubiquitous lithium-ion battery, but it uses sodium ions (Na+) as the charge carriers rather than lithium ions (Li+).

1.3.1. Principle

The working principle of a SIB is similar to that of the lithium-ion battery, which uses the embedding and stripping process of sodium-ion between positive and negative electrodes to realize charge and discharge. Na^+ is separated from the positive material and embedded into the negative material through the electrolyte during charging.

Electrons are transferred to the negative through the external circuit to maintain charge balance. On the contrary, Na^+ is removed from the negative electrode and embedded into the positive electrode through an electrolyte.

Under normal charge and discharge conditions, the insertion and removal of sodium-ion between the positive and negative electrodes do not damage the basic chemical structure of the electrode material. Sodium maintains a stable ionic form throughout the cycle of falling off and embedding. Sodium ions can cause chimera or swing at the battery's two poles, also called "Rocking chair battery". **[8]**

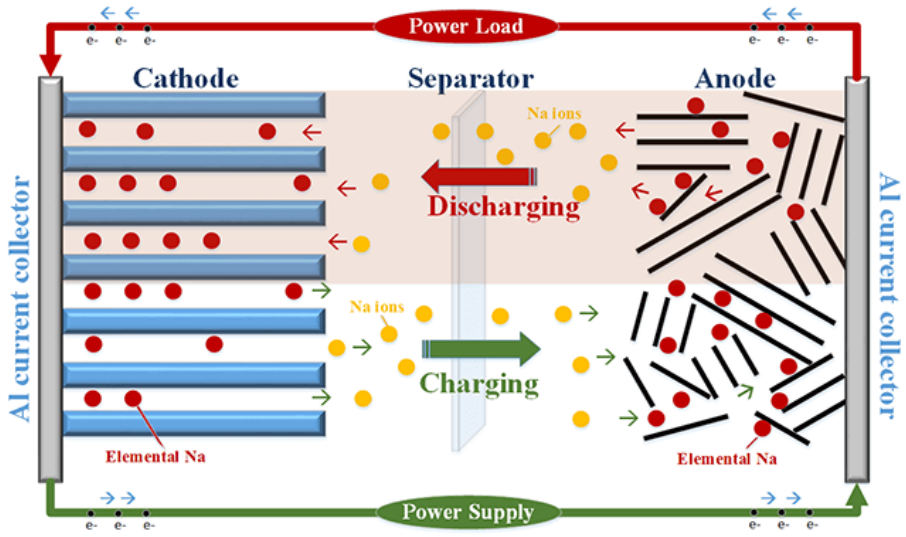

Figure 1.9. Schematic diagram of working principle of SIB's

When the battery is being charged, Na atoms in the cathode release electrons to the external circuit and become ions which migrate through the electrolyte toward the anode, where they combine with electrons from the external circuit while reacting with the layered anode material. This process is reversed during discharge.

1.3.2. Anode materials for SIB's

The negative electrode forms the lowest potential electrode. In a SIB, as solvated sodium ion works as the primary charge carrier, the thermodynamically lowest electrode potential is produced by the sodium reduction potential. To increase the battery's energy density, a negative electrode with theoretically the lowest potential and highest specific capacity is required.

Some of the anode materials are listed below:

- **Carbon-based anode materials**

The most used anode material in battery technology is graphite, which could not intercalate sodium to any appreciable extent and is electrochemically irreversible with low capacity and irreversibility of a Na/C (graphite) cell.

- **Metal oxide anode materials**

Metal oxides (MOx) and metal sulfides (MSα), especially layered metal disulfides, are used as anode materials based on conversion reactions. In most cases, the conversion reaction is accompanied by an intercalation or alloying reaction during the sodium insertion process.

- **Alloy-based anode materials**

Tin (Sn) and Antimony (Sb) is a promising alloy anode for Na-ion batteries. Sb performs better as an anode in Na-ion batteries than in Li-ion batteries, which is due to the formation of an amorphous intermediate phase. Na_3Sb.

1.3.3. Cathode materials for SIB's

- **Metal oxides MO_x**

Metal oxides MO_x are considered as SIB cathode alternative due to the low cost of the experiment and good electrical conductivity compared with others. Sodium-free MO_x cathode materials can also show incredible electrochemical properties related to specific capacity, rate capability, and cycling stability.

- **Layered oxides**

Layered oxide compounds, which are of interest as cathode materials for SIB, often have a formula Na_xMO_2, where M is referred to as different types of transition metals such as Cr and Mn.

- **Polyanion phosphate compounds**

Compared with monoanionic compounds, the redox potential of transition metals in polyanionic phosphates can be adjusted by the ionic covalent properties of OM bonds and polyanions (PO_4^{2-}) that move metal redox pairs (such as Fe^{3+}/Fe^{4+}) and presents a higher working voltage. Regarding the success of lithium-ion batteries, polyanionic phosphate compounds have also been considered as cathode materials for SIBs. They usually have the advantages of high structural stability and diversity, high operating potential, thermal safety, and excellent cycle performance due to the highly negative anions themselves.

  - **Sodium Vanadium Phosphate:** $NaVOPO_4$, a representative electrode material for sodium super-ion conductor, has good application prospects due to its good structural stability, high ion conductivity and high platform voltage (~3.4 V), **[9]**

- **Cathode material comparison**

Despite the low working potential, transition metal oxides can provide a specific capacity with an attractive specific energy of up to 600 $Wh \cdot kg^{-1}$. However, the oxide cathode's cycle stability and rate performance still require further improvements due to the inevitable lattice expansion and multiphase transition. Phosphate has good cycle stability, but the low specific capacity limits its performance.

1.3.4. Electrolyte

SIBs generally use $NaPF_6$ or $NaClO_4$ as sodium salt and carbonate as the organic solvent. This kind of electrolyte has been successfully matched with various positive and negative materials of SIBs and shows good comprehensive performance. In addition, liquid electrolytes also generally have potential safety hazards such as liquid leakage and combustion. For the relatively mature liquid electrolyte of SIB, further attention should be paid to the interface of its electrode process.

1.3.5. Applications of sodium-ion battery

Sodium-ion batteries can be used to power virtually any application that currently relies on lithium-ion batteries, some of the applications are listed below:

- **Automotive:**

  With EV sales expected to skyrocket over the next few years, sodium-ion technology is the obvious better choice because not only are they cheaper, which will make EVs more accessible, but they're also cleaner, lighter, and more stable.

- **Power grids:**

  Smart grids rely on reliable power, meaning an intermittent power supply can cause them to malfunction. Sodium-ion batteries could be used to optimize solar and wind energy to meet grid energy storage requirements.

- **Industrial mobility:**

  The properties of sodium-ion batteries mean that they can be used to maximize asset utilization and reduce operating costs with a constant state of readiness and high peak power.

1.3.6. Future of sodium-ion technology

Sodium-ion battery technology has benefitted from huge amounts of recent research activity, with developments in the space being particularly rapid due to their similarity to lithium-ion battery systems.

With recent discoveries such as hard carbon as a more suitable anode material and increasing demand in large-scale electrical energy storage, progress towards the commercialization of sodium-ion batteries is gaining traction. **[10]**

1.4. Objective

- To achieve single phase $NaVOPO_4$
- To evaluate the performance Sodium Vanadium hosphate (NVP)
- To study the influence of Di (Cu^{+} , Zr^{+}) and Tri valent (La^{+3}, Ti^{3+}) dopants in $NaVOPO_4$ over electrochemical performance.

1.5. Methodology

- To synthesize pure $NaVOPO_4$ through sol-gel method.
- To incorporate Cu^{2+}, Zr^{2+}, La^{3+}, Ti^{3+} in $NaVOPO_4$
- To characterize the pure and doped $NaVOPO_4$ for structural formation of monophase and evaluate the electrochemical performance

REVIEW OF LITERATURE

CHAPTER II

REVIEW OF LITERATURE

Sodium-ion batteries (SIB's) are considered one of the most promising alternatives to Lithium-ion batteries (LIB's) owing to the low cost and wide abundance of sodium. Sodium Vanadium Phosphate (NVP) is an attractive high-potential cathode material for Sodium-ion batteries. Phosphate compounds are promising materials for sodium-ion batteries because of their high structural stability. There are extensive researches that are ongoing based on their structure and application in energy storage devices. NVP is synthesized by various techniques such as hydrothermal technique, solid-state reaction, sol-gel method, carbo-thermal reduction method, etc., and the crystalline structure was characterized by the X-Ray diffraction technique. A broad review of literature summarizes the recently reported NVP based cathode materials for SIB applications.

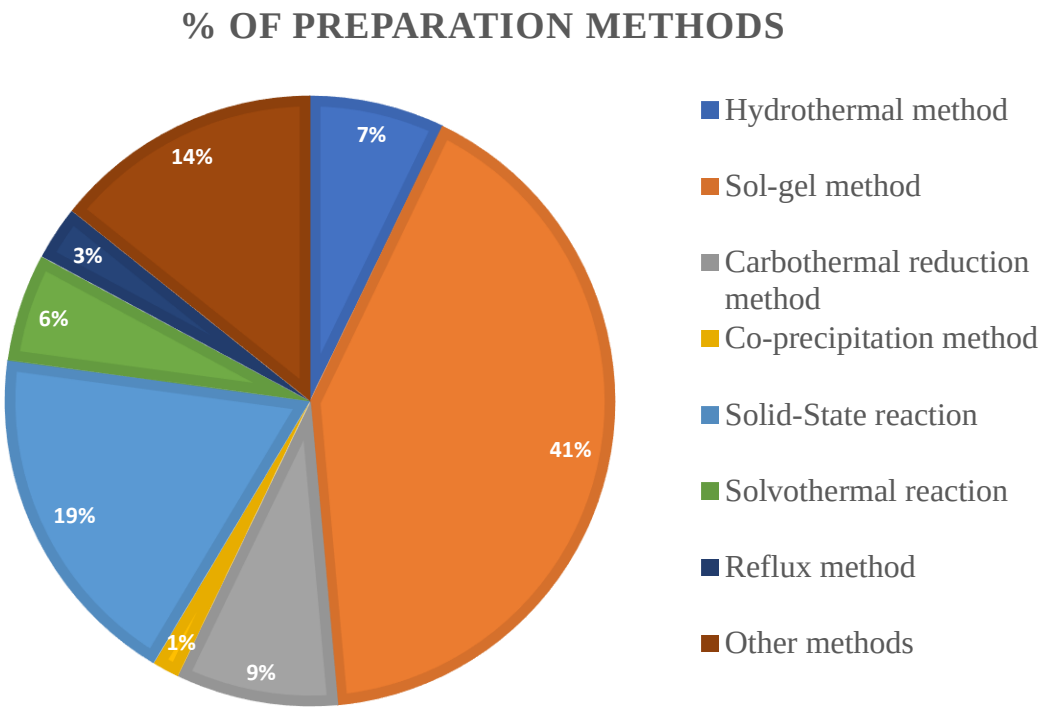

Figure 2.1. Pie-chart of review percentage based on preparation methods of NVP cathode for SIB's

2.1. Review Based on the Composition of $NaVOPO_4$

2.1.1. Based on the Composition of $NaVOPO_4$

[11] El abadila Iffer *et al.*, (2020) have reported the monoclinic α-$NaVOPO_4$ as cathode materials prepared by sol-gel method. In this paper, $NaVOPO_4$ has been used as a cathode material for sodium-ion battery. The single phase of monoclinic α-$NaVOPO_4$ structure with space group $P_{21/c}$ confirmed by the XRD analysis. The CV have one oxidation peak around 3.358 V in the potential range of 1-4.5 V vs Na/Na^+. At 0.05 C in room temperature, the cathode material gives a low reversible capacity of about 21 mA h g^{-1} when its discharge capacity decreases and the current rate increases. Therefore, the paper reports that monoclinic $NaVOPO_4$ exhibits poor performance i.e., caused by the high transfer charge resistance for sodium-ion batteries.

[112] Prashanta Mukharjee *et al.*, (2019) have reported that $NaVOPO_4$ prepared by the conventional solid-state reaction and a theoretical study has been carried out. A new spin-$\frac{1}{2}$ quasi-1D compound called $NaVOPO_4$ reveals the magnetism of a spin-$\frac{1}{2}$ alternating chain with a weak alternation of exchange couplings. This compound is well described by an alternating spin chain model with a dominant AFM (Atomic Force Microscopy) exchange coupling of J/kB 39 K and a minute spin gap of 0/kB 2 K. $NaVOPO_4$'s magnetic susceptibility might be consistent with the gapless uniform spin chain hypothesis. $NaVOPO_4$ is very close to the quantum critical point because of its weak alternation of exchange couplings and narrow spin gap.

[13] Pablo Aparicio *et al.*, (2018) reported $NaVOPO_4$ polymorphs as cathode materials for sodium-ion batteries. Vanadium Phosphate shows the high energy densities as cathode materials in sodium-ion batteries and Na-ion diffusion coefficients takes between 10^{-11} to 10^{-12} cm^2 s^{-1}. The Na^+ cations is surrounded by six atoms with Na-O distance from 2.23 to 2.36. α-, β- and α_1 $NaVOPO_4$ polymorphs shows the 1.3 x 10^{-11}, 6.7 x 10^{-12}, 5.7 x 10^{-11} cm^2 s^{-1} as the diffusion coefficients at 300 K. Three polymorphs show the cell voltage of 3.3, 3.1, 3.1 V. $NaVOPO_4$ acts as the superior cathode material because of its good electrochemical performance for sodium-ion batteries.

[14] Guang He *et al.*, (2016) have reported $NaVOPO_4$ has been prepared by sol-gel method. $NaVOPO_4$ acts as a cathode material. $NaVOPO_4$ have high theoretical capacities of 145 mA h

g^{-1} at 3.3 V. The energy density of $NaVOPO_4$ is 585 W h kg^{-1} is high due to the high theoretical capacity. The synthesized cathode material helps to improve the electronic and ionic conductivities by optimization.

[15] Chih-Yao Chen *et al.*, (2015) have reported sodium Vanadyl Phosphate ($NaVOPO_4$) been synthesized by sol-gel method. $NaVOPO_4$ has an infinitely long structure made of VO_6 octahedra joined by PO_4 tetrahedra, all of which share corners. With the NVP-2h and NVP-8h, the maximal capacity measured at 5 mA g^{-1} is maintained at 5 C and 10 C, respectively. The discharge capacity is still clearly discernible up to a rate of 40 C (5800 mA h g^{-1}). At 298 and 363 K, the $NaVOPO_4$ electrode displays a reversible capacity of 60 mA h g^{-1} and 101 mA h g^{-1}. These findings show NaVOPO4's promise for high-power applications, although more enhancements and electrode formulation modification are needed.

[16] Jie Song *et al.*, (2013) have studied the monoclinic $NaVOPO_4$ phase prepared by sol-gel method. The theoretical capacity of $NaVOPO_4$ is 145 mA h g^{-1}. As-synthesized particle size of $NaVOPO_4$ in the range of 20-30μm; after ball milling with carbon high energy is obtained and particle size were reduced to <2μm. The non-ball milled $NaVOPO_4$ gives a low reversible capacity of 20 mA h g^{-1} and the ball-milled $NaVOPO_4$ to give a reversible capacity of 90 mA h g^{-1} with the voltage range of about 2.0-4.4 V at the current density 1/15 C. The average potential of Na is 3.6 V.

2.1.2. Based on the composition of fluorinated $NaVOPO_4$

[17] Kiran Kumar *et al.*, (2021) had investigated the reflux method has been used to synthesize the cathode material $NaVOPO_4F$. $NaVOPO_4F$'s sharp diffraction peaks at 20.1, 23.9, 28.8, 32.0, and 35.6° can be attributed to the crystallographic planes (020), (211), (131), (300), and (013). The carbon layer is coated to the NVPF, sample to get higher electronic conductivity and the NVPF, particles are soft carbon in nature and crystallinity. Pure NVPF, 10-SC@NVPF, 15-SC@NVPF, and 20-SC@NVPF electrodes have Na-ion diffusion coefficients of 4.66 10^{-15}, 9.2 10^{-15}, 4.59 10^{-14}, and 1.82 10^{-14} cm^2 s^{-1}, respectively. The 15-SC@$NaVPO_4F$ composite electrodes provide a reversible initial capacity of 109 mA h g^{-1} during the second cycle and maintain 95% of the capacity at the end of 300 cycles at 0.1C. They also maintain 77% (81 mA h g^{-1}) capacity retention after 1000 cycles when taking into account the initial capacity of 105 mA h g^{-1} at 0.5C. NVPF cathode also shows an operating voltage of about 3.3 V. $NaVPO_4F$ cathode material has the potential for practical applications to form sodium-ion batteries.

[18] Chen-De-Zhao *et al.*, (2020) have reported that $NaVPO_4F$ synthesised through a feasible two-step solid state carbon thermal reduction (CTR) method. NaVPO4F throughout the subsequent steps of sodiation and desodiation, improves cycling stability. $NaVOPO_4F$ are combined with reduced graphene oxide (rGO) composites and the discharge capacity of the NVPF@5%rGO electrode is 96.6, 95.4, 89.4, 80.5 to 70.3 mA h g^{-1}, which is higher than the corresponding values of NVPF (82.7, 81.1, 77.8, 66.5 and 56.5 mA h g1 at 0.1, 0.5, 2, 10 and 20C, respectively), and it also exhibits the best rate capabilities than other materials. The reversible capacity still has an 82.71% capacity retention after 1500 cycles, showing a relatively minor fading of 0.0115% per cycle. As a result, the synthesised NVPF@5%rGO demonstrates the anticipated excellent electrochemical performance when employed as a cathode for Sodium half cells.

[19] Xiaochen Ge *et al.*, (2018) synthesized $NaVOPO_4F$ composites by one-step facile solution method with uniform carbon coating layer ($NaVOPO_4F$/C) and PVP ($NaVOPO_4F$/C) is used as a chelating agent. From the Raman spectra, two peaks are observed around 1340 cm^{-1} and 1578 cm^{-1} which attributes for NVPF/C-PVP to the D-band and G-band carbon coating layer. The electronic conductivity of NVPF/C-PVP is $4.2x10^{-2}$ which is higher than the NVPF/C. NVPF/C-PVP cathodes shows a high electrochemical performance as 68 mA h g^{-1} at 20 C. After 1000 cycles at 10 C, it shows a retaining capacity of 81.8%.

[20] Markas law *et al.*, (2018) have synthesized $NaVOPO_4F$ (NVPF) by one-step soft template method. Vanadium (III) oxide (V3-NVPF) and vanadium (V) oxide (V5-NVPF) are used as precursors. Na-ion fuel cell has a discharge voltage at 3.7 V with an initial discharge capacity at 0.1 C is 79 mA h g^{-1}. The NVPF half-cell has the sodium storage capacity of about 124 mA h g^{-1} for the V3-NVPF 133 mA h g^{-1} for the V5-NVPF at 0.1 C. At 0.1 C, as compared to V3-NVPF, V5-NVPF initial discharge capacity is higher. V5-NVPF is capable of 2,500 cycles at 1 C having high discharge capacity with 82% retaining capacity and V3-NVPF have only 52% retaining capacity after 2,500 cycles. This study explains that sodium-ion battery cathode material gives unique properties for sodium storage performance and long-term cycling stability.

[21] Pingyuan Feng *et al.*, (2018) reported $NaVOPO_4F$ prepared by sol-gel method for high performance electrode in SIBs. From the XRD patterns, the obtained porous 3D coral structure of NVPF exhibits a relatively large surface area which is providing a surfacient contact interface. NVPF calcinated at 750˚C for12 hours (NVPF-750-12) obtained a highest initial

discharge capacity of 106 mA h g^{-1} at 2 C. A reversible capacity of 100 mA h g^{-1} is released by the cathode at 5 C, which is extremely near to the capacity at 1 C rate. The NVPF-750-12 provides 88 mA h g^{-1} even at 50 C, and the capacity retention at 5 C may maintain over 70% after 2500 cycles. Other fluorine-containing polyanion-type materials for Sodium-ion batteries and Lithium-ion batteries can be manufactured using this simple approach and efficient synthetic route for building 3D specific structures.

[22] Barker *et al.*, (2003) have successfully investigated the sodium-ion based Fluorophosphate compound $NaVOPO_4F$ prepared by a solid-state reaction. XRD pattern shows the broadness of the peak with a random distribution of carbon-carbon layers in the material. The average discharge voltage for sodium-ion cell was determined to be about 3.7 V as on cathode materials. The specific capacity for cathode is 82 mA h g^{-1} and 202 mA h g^{-1} determined for Fluorophosphate and hard carbon active materials. $NaVPO_4F$ have been used as the commercially hard carbon material.

2.1.3. Based on the composition of carbonated $NaVOPO_4$

[23] According to **Yongjin Fang *et al.*, (2021),** the fabrication of Na containing amorphous cathode material, amorphous $NaVOPO_4$ when dispersed on the reduced graphene oxide (a-NVOP@rGo) has been synthesized by facile reflux reduction method. The average working potential of the a-NVOP@rGO microflower electrode was 3.5 V, which was higher than that of $NaFePO_4$. The discharge capacity of a-NVPO@rGO is 110 mA h g^{-1} and higher rate relative to a high energy density of about 383 W h kg^{-1}. At 0.05, 0.1, 0.2, 0.5, 1, 2, and 5 C, the electrode can give an average reversible capacity of 108, 90, 81, 70, 65, 58 and 50 mA h g^{-1}. A new path for cathode performance, particularly for the polyanion-type cathode, could be opened up by research on this novel amorphous $NaVOPO_4$ cathode, which has intrigued electrochemical properties and a distinctive Na-storage mechanism. This would help advance the commercialization of sodium-ion batteries in the future.

[24] Yongjin Fang *et al.*, (2018) reported simple solvothermal reduction process that have been used to synthesize $NaVOPO_4$ and $NaVOPO_4$/C as a cathode material. Raman Spectra of $NaVOPO_4$ exhibits Raman patterns with symmetric stretching vibrations of PO_4 at about 937 cm^{-1} and stretching vibrations of V=O bonds at 990 and 1,029 cm^{-1}. The average discharge potential of the $NaVOPO_4$/C cathode is 3.5 V, which is higher than that of conventional metal oxide cathodes. The $NaVOPO_4$/C electrode's discharge capacity reaches 144 mA h g^{-1} at 0.05

C, which is equivalent to $NaVOPO_4$ full theoretical at $1e^-$ redox capacity of 145 mA h g^{-1} and strong rate capability at 5 C. The energy density of $NaVOPO_4$ is 504 W h kg^{-1}. The facile synthetic procedure produced in this work can be readily applied to additional alkali-metal intercalation cathodes for a variety of energy storage and used for conversion applications.

[25] Yang Ni *et al.*, (2018) have reported that β-$NaVOPO_4$ has been synthesized by a microwave-assisted solvothermal method and the β-$NaVOPO_4$/C has been prepared by ball-milling method. The ball-milling procedure increases the diffusion coefficient of Na-ions from 2.36 x 10^{-15} cm^2 s^{-1} to 1.05 x 10^{-14} cm^2 s^{-1} for β-$NaVOPO_4$/C. The resulting electrodes have a reversible capacity of 80 mA h g^{-1} and a clearly defined plateau at 3.3 V vs Na/Na^+. The discharge capacities are increased to 115 mA h g^{-1} for $NaVOPO_4$/C at a high temperature of 45˚C. Thus, the cathode material has the potential to exhibit the good practical applications upon structural optimization.

2.2. Review Based on the Composition of $Na_3V_2(PO_4)_3$@C

[26] Hou Baoxiu *et al.*, (2021) reported 3D porous $Na_3V_2(PO_4)_3$/C prepared by the simple sol-gel method. In this study, $Na_3V_2(PO_4)_3$/C is used as a high-performance cathode material for Sodium-ion Batteries. XRD of NVP sample shows the rhombohedral structure. From the Raman spectra, the peaks are observed at 1349 and 1592 cm^{-1} for the D bands and the G bands. The molar mass of citric acid is considered to be low because the citric acid shows the poor electrochemical performance due to a high proportion of carbon in materials. The rate capability of NVP/C with 0.21 g of citric acid is extremely high. NVP/C has a specific capacity of 115.7, 105.7, 100.6, and 91.3 mAh g^{-1} at current rates of 1, 5, 10, and 20 C, respectively. Even at a high current rate of 50 C, a specific capacity of 74.4 mAh g^{-1} is achieved. Therefore, NVP as a cathode material for Sodium-ion batteries has been considerable interest due to its unique advantages.

[27] Xiaohong Liu *et al.*, (2020) reported $Na_3V_2(PO_4)_3$ prepared via sol-gel method by simultaneous carbon coating and Nb^{+5} doping. A combined technique of carbon coating and Nb^{+5} doping has been carried for the first time and the carbon coated nano-shell might create an electron-conductive network and buffer the volume strain. The specific surface area of the Nb-0, Nb-0.2 and Nb-0.3 samples is calculated to be 18.91, 28.2, 34.62, 8.04 m^2 g^{-1} according to nitrogen adsorption-desorption isotherms for all samples. Nb-0, Nb-0.1, Nb-0.2 and Nb-0.3 have measured electron conductivities of 4.54 x 10^{-3}, 6.29 x $10^{-3,}$ 1.72 x 10^{-2} and 5.08 x 10^{-2-} S

cm^{-1}. When Nb-0.2 sample is optimized, the specific capacity decreased from 101.4 mA h g^{-1} to 81.6 mA h g^{-1} when the current densities increased from 0.1 C to 50 C for a preferable rate performance. This study says that the enhanced intrinsic electron conductivity and structural stabilization brought on by super valent element replacement may point to a feasible technique for producing alternative polyanion cathode materials.

[28] Nali li *et al.*, (2020) reported sol-gel method is used for the preparation of $Na_3V_2(PO_4)_3$ as a cathode material for sodium ion batteries. The rate performance was improved with the creation of 3D electronic conductive network on the NVP using a thin and uniform carbon layer. The initial discharge capacities for NVP@C are 114.4, 116.8, 118.0 and 117.5 optimised when the carbon content is increased. NVP/C had an initial capacity of 64.4 mA h g^{-1} and a final capacity of 52.5 mA h g^{-1} after cycling, with a capacity retention of 81.5%. The absorption is taken place for different level of carbon content i.e., NVP/C-G. The reversible capacity of 52.5 mAh g^{-1} at 10 C with an initial capacity of 64.4 mA h g^{-1} exhibited for NVP/C-G10% composite after 1000 cycles. This method provides a facile and efficient method for synthesizing a 3D interconnected porous NVP/C cathode with high electrochemical performance for Sodium-ion Batteries.

[29] Qizhen Zhu *et al.*, (2019) reported nano porous $Na_3V_2(PO_4)_3$ (NVP@pC) have prepare by the sol-gel method with the assistance of a hierarchical porous carbon. The porous carbon framework improves the electrical and ionic conductivity for efficient charge transport, while the nano-NVP provides fully exposed active sites, short diffusion lengths and minimum volume change. The theoretical capacity of the NVP ($Na_3V_2(PO_4)$) is 117 mAh g^{-1}. The pore volume of the nano-NVP@C-3 is 0.56 cm^3 g^{-1}, and it has a specific surface area of 430 m^2 g^{-1}. The pristine NVP cathode has an initial capacity of 86.9 mAh g^{-1}, while the nano-NVP@pC-1, nano-NVP@pC-2 and nano-NVP@pC-3 cathodes have initial capacities of 112.8, 113.5 and 116.2 mAh g^{-1}, respectively. The reversible capacities of the nano-NVP@pC-1, nano-NVP@pC-2 and nano-NVP@pC-2 cathodes 47.2, 70.1 and 89.5 mAh g^{-1} at 20 C. In comparison to NVP cathode, nano-NVP@pC-3 cathode exhibits a higher capacity of 116.2 mAh g^{-1} at 0.2 C and gives a high rate in sodium-ion storage performance. The nano-NVP@pC becomes a promising cathode material for high power Sodium-ion Batteries by this simple preparation method. From this study, it is clear that, it is possible to create active materials for different energy storage devices, including supercapacitors and other secondary batteries in a porous carbon framework.

[30] Hyeongwoo Kim *et al.*, (2019) has worked on the polydopamine-derived N-doped carbon-wrapped $Na_3V_2(PO_4)_3$ cathode synthesized by simple sol-gel method. TG-DTA curves have obtained in the temperature range of 25-800 ˚C. Initial discharge capacities for NVP and NC@NVP are 104.1 (94.91 $mAhg^{-1}$ at room temperature) and 116.7 $mAhg^{-1}$ (101.0 $mAhg^{-1}$ at room temperature), respectively. With a high discharge capacity of 107.3 mA/hg^{-1}, NC@NVP exhibits outstanding capacity retention at high temperatures, which is 92.0% at the 500th cycle. The polydopamine-derived N-doped carbon-wrapped NVP is expected to be a novel cathode material for sodium-ion batteries. It is also envisaged that the N-doped carbon precursor can be practically used in surface modification for large-scale sodium-ion batteries.

[31] Yanjun Chen *et al.*, (2018) reported Al doped NVP@C have prepared by the carbon-thermal reduction method. Carbon coating can improve the electrochemical performance both in Sodium-ion batteries and Lithium-ion batteries. The samples prepared containing 1%, 2% and 3% Al-doping can be abbreviated as NVP-A10, NVP-Al1, NVP-Al2 and NVP-Al3, respectively. NVP-Al0, NVP-Al1, NVP-Al2 and NVP-Al3 exhibits the initial discharge capacities of 100.2, 99.8, 102.7, 96.7 mA h g^{-1} at 10 mA h g^{-1} and coulombic efficiency of 92.8%, 92.3%, 90.5%, 91.9% respectively. The NVP-Al2 shows the best rate performance and the discharge capacities of NVP-Al2 are 98, 92.7, 88.2, 83.9, 77.4, 66.1 mA h g^{-1} at 10, 20,50,70, 120, 200 mA h g^{-1}. The electronic conductivity of the samples NVP-Al0, NVP-Al1, NVP-Al2, NVP-Al3 are 4.47 x 10^{-4}, 6.98 x 10^{-4}, 9.83 x 10^{-4}, 1.18 x 10^{-4} s cm^{-1}. NVP-Al2 material exhibits an initial discharge capacity of 102.7 mA h g^{-1} at 10 mA g^{-1} and have a discharge value of 95 mAh g^{-1}. Through Al-doping, the electrochemical performance can be enhanced to the structural stability and high Na^+ ion conductivity that has been confirmed by the XRD analysis. Hence, this study concludes that Al-doping material would be a promising cathode for energy storage device.

[32] Yanli Ruan *et al.*, (2018) reported the hydrothermal method is used for the preparation of NVP@C When the current rate is changed from 0.05, 0.1, 0.5, and 1 to 2 C, the discharge capacity decreases slightly from 117.4, 116.6, 114, and 112.4 to 109.5 mAh g^{-1}. The initial discharge capacity of NVP/C is 106.8 mAh g^{-1} at a rate of 5C. The reversible capacity of 115.7 mAh g^{-1} can be maintained when the current rate drops to 0.05 C, demonstrating the NVP/C nanosheets' exceptional rate performance. The first discharge capacity has a 90% coulombic efficiency and is to be 101.3 mAh g^{-1}. This NVP/C-based symmetric cell has a reversible discharge capacity of 85mAh g^{-1}, an average voltage of 1.7 V at a rate of 1 C, and 96.4%

capacity retention after 100 cycles. An innovative concept for creating high-performance room-temperature sodium-ion cathode materials is discussed in this study.

[33] Hezhang Chen *et al.,* (2018) have reported Reduced Graphene Oxide Decorated $Na_3V_2(PO_4)_3$ prepared by spray drying method of Hummers Methods from Nature Flake Graphite. The discharge capacities of the NVP/G8 electrode are 102.2, 100.7, 98.1, 90.8, 85.8, 82.3, 78.5 and 72.0 mAh g^{-1} at 0.2, 1, 5, 20, 30, 40, 50 and 60 C. Even at 70 C, the electrode continued to exhibit a discharge capacity of 64 mAh g^{-1}. The capacities of the NVP/C electrode, in comparison, are 112.3, 105.6, 98.8, 92.6, 87.0, 80.0, 73.1 and 66.8 mAh g^{-1} at 0.2, 1, 5, 10, 15, 20, 25 and 30˚C. A promising Cathode material to achieve greater electrochemical performance for energy storage is proved to be NVP microspheres decorated with rGO sheets.

[34] Yilin Zhao *et al.,* (2018) reported Carbon-coated $Na_3V_2(PO_4)_3$ Nanoflakes (NVP/C) have prepared by Solid-state reaction for High-Rate Capability and Ultralong Cycle-Life Sodium Ion Batteries. The theoretical capacity of NVP is 117.6 mA h g^{-1}. NVP nanoflakes have an initial charge capacity of 115.3 mA h g^{-1}, which is close to their theoretical capacity. With discharge capacities of 114.2, 112.3, 105.3, 101, 98.1 and 95.3 mA h g^{-1} at varied current densities of 0.5, 1, 2, 5, 10, 20 and 50 C, the NVP nanoflakes exhibit exceptional rate performance. A reversible capacity of 87.7 mA h g^{-1} is attainable even at an ultrahigh rate current density of 100 C. NVP can deliver a high discharge capacity of 114.5 mA h g^{-1}, when the current density was reset to 0.5 C. The initial specific discharge capacity is 100.3 mA h g^{-1}, and the capacity remains at 52.5 mA h g^{-1} after 10,000 cycles, with capacity retention of 52.3% and the capacity fading of 0.0048% per cycle. According to the research exists, the hierarchical porous carbon-coated NVP nanoflakes electrodes showed good sodium storage performances, including a high reversible capacity of 114.2 mA h g^{-1} at 0.5 C and a high-rate capacity of 87.7 mA h g^{-1} at 100 C. As a result, the hierarchical porous carbon-coated NVP nanoflakes electrodes exhibit high reversible capacity, high-rate capability, and outstanding cyclic stability as a cathode material for Sodium-ion Batteries.

[35] Xiaohong Liu *et al.,* (2018) reported $Na_3V_2(PO_4)_3$/C as a cathode material and it is prepared by solid-state reaction method. XPS measurement shows the surface chemical composition of NVP@C and it consists of Na, V, P, O and C elements. The specific area of NVP@C1, NVP@C2 and NVP@C3 determined by BET technique and the values are 60.13 m^2 g^{-1}, 31.3 m^2 g^{-1} and 27.20 m^2 g^{-1} respectively. At 0.1 C, the initial discharge capacity of NVP@C is 108 mA h g^{-1} which is nearer to its theoretical capacity of 117.6 mA h g^{-1}. At 0.2,

0.5 1, 3, 5, 10, 20 and 30 C, the notable reversible capacities are 105, 102, 100, 98, 97, 95, 88, 81 mA h g^{-1}. Specifically, the initial discharge capacity for NVP@C1, NVP@C2 and NVP@C3 are 99, 104, 104 mA h g^{-1} obtained. The capacity of NVP@C3 have a high capacity of 86 mA h g^{-1} even after 1000 cycles and the capacity retention is 82.8%. Meanwhile, the NVP@C3 composite's cycle performance is measured at 5 C; its initial capacity is 96 mA h g^{-1}, and it also shows a high-capacity retention value after 500 cycles as 95.9%. The NVP@C3 composite shows a superior electrochemical performance than NVP@C1 and NVP@C2. In this study says, the carbon coating approach will increase the electrochemical performance in batteries and it will be useful for accelerating the commercialization of Sodium-ion Batteries.

[36] Zifan Zhou *et al.*, (2018) have successfully synthesized the $Na_3V_2(PO_4)_3$ nanoparticles encapsulated in carbon nanofibers through a facile electrospinning method and subsequent calcination. It has been used as a cathode material in sodium-ion batteries. Raman spectrum shows peaks at 1342 cm^{-1} and 1608 cm^{-1} of D and G-bands. The initial discharge capacity of the nanofiber cathode is around 110.6 mAh g1, which is 93.7% of its theoretical capacity. It can still deliver a reversible capacity of 106.7 mAh g^{-1} even after 50 cycles with a capacity retention of 96.5%. At 0.2, 0.5, 1 and 2C, the synthesized $Na_3V_2(PO_4)_3$@C electrode can have specific capacities of 108.1, 105, 100.4 and 94.7 mAh g^{-1}.

[37] Ling Wu *et al.*, (2018) reported $Na_3V_2(PO_4)_3$ have prepared by a pre-reduction assisted electrospinning method. Here in this report, $Na_3V_2(PO_4)_3$ is used as a cathode material in Sodium-ion batteries. At 0.05 C rate, the NVP sample exhibited a discharge capacity of about 114.0 mAh g^{-1} close to the theoretical capacity and even at 10 C, it still maintains a capacity of 77.9 mAh g^{-1}. Under the optimum synthesis conditions of 800˚C, 10 h and heating rate of 2.5 ˚C min^{-1}, the obtained $Na_3V_2(PO_4)_3$/C composite nanofibers present excellent electrochemical performances.

[38] Ling Wu *et al.*, (2018) have studied the room-temperature pre-reduction of spinning solution for the synthesis of $Na_3V_2(PO_4)_3$/C (NVP/C) nanofibers as high-performance cathode materials for Sodium-ion batteries. NVP/C nanofibers was prepared by electrospinning method after pre-reduction of spinning solution at room temperature. XRD patterns shows rhombohedral structure with R-3C space group. At current densities of 0.1, 0.2, 0.5, 1, 2, 5 and 10C, the discharge capacities can reach 113.0, 110.3, 107.8, 106.1, 102.2, 93.2 and 78.1 mAh g^{-1}. the Thus, the impressive electrochemical performances of $Na_3V_2(PO_4)_3$/C, especially the high-rate capability, can be successfully achieved.

[39] A sol-gel assisted hydrothermal method has been used for the preparation of $Na_3V_2(PO_4)_3$ (PL-NVP@C and NVP@C) is reported by **Enhui Wang *et al.*, (2017)** Na-ion transfer and inter-facial electrical conductivity are improved by the carbon layer coated on the NVP. In comparison to NVP@C, which has a specific surface area of 33.1 m^2g^{-1}, the PL-NVP@C is found to have a specific surface area of 64.9 $m^{-2}g^{-1}$. At current densities of 1, 3, 5, 10, 20, 30, 40 and 50 C, the discharge capacities of 110, 109, 107, 104, 101, 97, 94 and 92 mA h g^{-1}. The discharge capacity has been maintained as high as 84.5% within 72s even when the current densities reach at 50 C. After 300 cycles at 1C and comprehensive Na-ion extraction and insertion, PL-NVP@C still has 98.6% of its initial capacity. Outstanding rate performance (92 mA h g^{-1-} at 50 C) and cycling stability (91.3% retention after 2000 cycles at 10 C) are exhibited by the PL-NVP@C composite. This study of NVP@C would be beneficial for the synthesis of other carbon-based composite materials which needs particle size reduction and conductivity promotion.

[40] M.J. Aragon *et al.*, (2017) reported $Na_3V_2(PO_4)_3$/C synthesized by citric based Sol-gel method. The use of conductive substances is necessary for sodium-ion batteries to use $Na_3V_2(PO_4)_3$ as an effective cathode. The presence of low or moderate amounts of carbon limits crystallite growth and reduces local strain and defects. The initial capacity increases when the carbon content increases and the values are 104.2, 106.7 and 101.7 mA h g^{-1} recorded for NVP-C2, NVP-C3 and NVP-C4 at C/2. Both NVP-C2 and NVP-C3 showed a similar rate capacity to 20C when the C rate is increased to 40 C, only NVP-C3 is able to maintain capacity values over 50 mA h g^{-1} at 40 C. At 2C, a full sodium-ion cell (Hard Carbon/NVP-C2) is able to deliver an energy density of up to 320 W h kg^{-1}. This carbon-optimized $Na_3V_2(PO_4)_3$/C composite is encouraged to be considered as a potential choice for the positive electrode of sodium-ion cells due to its good energy density.

[41] Shaonam Shi *et al.*, (2017) successfully investigated the $Na_3V_2(PO_4)_3$/C cathode material synthesized by normal temperature chemical reduction and sodiation method. In this, Oxalic Acid is used as both reducing agent and a carbon source. The specific capacity of the sample is 113.3, 109.5, 100.2, 82.9 and 58.5 mAh g^{-1} at current densities of 0.1A, 0.5C, 1C, 2C and 4C respectively. The sample's initial discharge capacity (114.9 mAh g^{-1}) at 0.05C rate is nearly equal to the theoretical capacity.

[42] Shiqi Sun *et al.*, (2021) have studied the structure of $Na_3V_2(PO_4)_3$/C@CNTs-WC synthesized by sol-gel route followed by freeze-drying process and used as a cathode material

for sodium-ion batteries. XRD pattern shows the monoclinic structure and no extra reflections has been noticed. From the GCD analysis, the initial discharge capacities of NVP for W0.0-NVP, W0.03-NVP, W0.05-NVP are95.2, 115, 102.2 and 110 mAh g^{-1} respectively. W0.01-NVP shows the highest initial capacity of 116 mAh g^{-1} maintained at 1C and it still maintains nearly 100 mAh g^{-1} even after 300 cycles. The advantageous wolfram doping could efficiently maintain the open NASICON structure of NVP and produce a huge number of advantageous holes to speed up electronic transportation. The wolfram doping and CNTs enwrapping to construct a multi-dimensional conductive framework is a prospective route for cathode materials with high performance in Sodium-ion batteries.

[43] Zeyi Tian *et al.*, (2021) reported boosting the rate capability and working lifespan of K/Co co-doped $Na_3V_2(PO_4)_3$/C cathode material for sodium-ion batteries. $Na_3V_2(PO_4)_3$ have been prepared by the sol-gel method. From the BET analysis, the $K_{0.1}Co_{0.05}$-NVP/C sample has a surface area of 13.805 m^2 g^{-1}. The interface contact between the electrode and electrolyte improved by the large specific area. The best capacity retention has been observed by $K_{0.1}Co_{0.05}$-NVP/C, whose reversible capacities are 117.1, 101.1, 97.9, 90.2, 85.6, and 111.2 mAh g^{-1} at various current densities. $K_{0.1}Co_{0.05}$-NVP/C cathode can deliver a high reversible capacity of 100.9 mAh g^{-1} and maintains 71 mAh g^{-1} after 500 cycles. Therefore, K/Co co-doping will be an efficient cathode material to improve the electrochemical performances in Sodium-ion batteries.

[44] Guo-dong Yi *et al.*, (2021) successfully investigated the N-doped $Na_3V_2(PO_4)_3F_3$/C cathode assisting by plasma enhanced chemical vapor deposition for sodium-ion batteries. $Na_3V_2(PO_4)_3F_3$/C was prepared by the one-step sol-gel method. XRD patterns shows a high crystallinity due to the strong peaks appeared at (220) and (222). Raman spectrum shows two vibrant peaks at 1327 cm^{-1} and 1592 cm^{-1} showing the presence of carbon. N-doped NVP exhibits a high conductivity magnitude of 3.75 x 10^{-2} S cm^{-1} which improves the electrochemical performances of cathode in sodium-ion batteries. A high capacity of 102.6 mAh g^{-1} at 10 C is released by N-doped NVP. After 100 cycles at 1 C, the capacity retention is as high as 96.5%. It also delivers an excellent cyclic performance in which 91.4% capacity are maintained after 1000 cycles.

[45] Nitheesha Shaji *et al.*, (2021) reported Nitrogen-doped Carbon Coated $Na_3V_2(PO_4)_3$ (NC/NVP) cathode for rechargeable sodium-ion batteries. NC/NVP have been prepared by using a simple and facile solution evaporation method. The materials are highly crystalline and

free of contaminants, as evidenced by the strong XRD peaks. In Raman Spectra, the peaks of NC/NVP are observed at 1350 cm^{-1} and 1600 cm^{-1} for D and G bands. The synthesized NC/NVP-MS displayed a specific discharge capacity of 114 m Ah g^{-1} at 0.1 C for the first cycle and maintained 107 mAh g^{-1} in the 100^{th} cycle with a capacity retention of 93.8% in the room temperature condition. The ability of the nitrogen-doped carbon layer coating on NVP to increase the electrical and ionic conductivity and consequently improve the overall electrochemical performance.

[46] Zhaoyang Wang *et al.*, (2020) synthesized $Na_3V_2(PO_4)_3$/C cathode material through Br and N co-doping by Sol-gel assisted hydrothermal method. The products were prepared with 0.1, 0.125, 0.15 g CTAB and it was denominated as Br/Na-C@NVP-1, Br/Na-C@NVP-2 and Br/Na-C@NVP-3 respectively. Among these samples, Br/N/a-C@NVP-2 exhibits the better performance and it shows the reversible capacity of 41 mA h g^{-1} at the current density of 10 C and retains a capacity of 80% after 500 cycles. Even at a high current density of 20 C, the reversible capacity is 22.9 mA h g^{-1} with 72% capacity retention after 1000 cycles. According to this research, Br and N cooping holds significant promise for producing battery electrodes with excellent electrochemical properties.

[47] Xiaoying Liu *et al.*, (2020) reported Carbon encapsulation and chlorine doping enable $Na_3V_2(PO_4)_3$ have prepared by Sol-gel method and it is used a cathode material for Sodium-ion Batteries. The electrical conductivity and the electrochemical properties were improved by forming the Carbon layer composite. When chlorine is doped with NVP, the discharge capacity increase and the decreased the content of doped chlorine. The best electrochemical performances are exhibited by the chlorine content of NVP@C/CL-30 composite. Specific reversible capacity for NVP@C/Cl-30 is 104.2, 86.4 and 52.2 mA h g^{-1} for current densities of 40, 1000 and 4000 mA h g^{-1}, respectively. These values are much greater than those for NVP@C composite (74.2, 46.4 and 21.1 mA h g^{-1}). The peak current densities for the oxidation and reduction processes of NVP@C/Cl-30 composite are substantially higher than those of NVP@C (0.142 A g^{-1} and 0.121 A g^{-1}). The initial discharge capacity of NVP@C and NVP@C/Cl-30 are 41.1 and 83.4 mAh g^{-1}. The discharge capacity of NVP@C/Cl-30 reaches 80.7 mAh g^{-1} which is higher than that of NVP@C (50.9 mAh g^{-1}) after 500 cycles. In conclusion, the electrical and ionic conductivity are increased by the Carbon encapsulation and chlorine doping.

[48] Jin An Sam Oh *et al.*, (2020) reported dual nitrogen-doped carbon decorated on $Na_3V_2(PO_4)_3$ to stabilize three sodium ions intercalation synthesized by facile intercalation process. Because to its high theoretical energy density and stable crystal structure, (NVP) is one of the most promising cathode materials for high-voltage sodium-ions batteries. The highest theoretical energy density of NVP is 400 Wh kg^{-1} when two Na ions being extracted from the lattice. NVP@C/rGO-U delivered a high discharge capacity of 107.86 mAh g^{-1} at 1 C with the capacity retention. All electrode materials (NVP@C, NVP@C/rGO and NVP@C/rGO-U) shows the high crystallinity with rhombohedral structure. Raman spectrum shows peaks at 1350 and 1605 cm^{-1} attributed to D-band and G-band. The NVP@C/rGO and NVP@C/rGO-U are estimated to have specific surfaces of 41 and 37 m^2 g^{-1}, respectively. At 0.5, 1, 3, 5, 10, 15, 20, 25 C, the reversible capacity of NVP@C/rGO-U are 107, 106, 103, 101, 97, 94, 91, 86 mAh g^{-1} respectively. NVP can still deliver 96 mAh g^{-1} at 5 C even at a higher mass loading and it implies a outstanding electrochemical properties. This study demonstrates that the simple synthesis technique offers a different perspective to the industrial manufacturing of high-energy-density SIBs with exceptional fast-charging capabilities.

[49] Jiahao Li *et al.*, (2020) reported K/Zr co-doped $Na_3V_2(PO_4)_3$/C have prepared by solid-phase method. XRD pattern shows the rhombohedral structure with R-3c space group. At the rate of 0.1C, the initial discharge capacity of NVP/C, KZ0.01, KX0.04, KZ0.07 AND KZ0.1 are 94.5, 91, 100.3, 107.3 and 97.1 mAh g^{-1} respectively. The discharge capacities of NVP/C at 0.1, 0.2, 0.5, 1, 5, 10 and 1C are 69.5, 64.1, 59.3, 56.8, 53.1, 49.0 and 65.5 mAh g^{-1}. The specific energy of the NVP/C composite is 241.3 Wh kg^{-1} which is much lower than that of co-doped composites. In this study, solid-phase method is used to enhance the bulk electronic conductivity and ionic conductivity.

[50] Linnan Bi *et al.*, (2020) extensively studied the modulation of the crystal structure and ultralong life span of a $Na_3V_2(PO_4)_3$ cathode for a high performance by Niobium-Vanadium substitution in Sodium-ion batteries. Nb^{5+} doped $Na_3V_2(PO_4)_3$ samples were prepared by solid-state method. XRD pattern reveals the crystalline structure of NVP/Nb as rhombohedral. Raman spectra shows peals at 1226 and 1450 cm^{-1} are associated with the carbon of sp^3. NVP/Nb-0.3 delivers the highest capacity of 113.7 mAh g^{-1} with a coulombic efficiency of 95.1%. It still produces a discharge capacity of 53.7 mAh g^{-1}, even after 4000 cycles, demonstrating its exceptional cycling characteristics. An important reference for improving battery performance is provided by this cathode material modification technique.

[51] Outstanding electrochemical performance of sodium vanadium phosphate cathode co-modified by carbon-coating and titanium-doping for Na-ion batteries reported by **Yu Gu *et al.*, (2019).** $Na_3V_2(PO_4)_3$ have prepared by simple carbon thermal reduction method. Before Titanium doping, the sample shows a reversible capacity of 105.3 mAh g^{-1} at 0.1C for the first cycle. After Titanium doping, the electrode shows a higher specific capacity than the Ti=0 electrode. The Titanium doped sample exhibits a higher specific capacity of 115.2 mAh g^{-1} at 0.1C. Even at 5C, a specific capacity of 106.3 mAh g^{-1} can still be reached, which is approximately 90.4% of its theoretical capacity (118 mAh g^{-1}). Carbon coated and doped titanium-ion can significantly improve $Na_3V_2(PO_4)_3$'s apparent and intrinsic electrical conductivities.

[52] Wei Li *et al.*, (2019) reported N-doped carbon-encapsulated $Na_3V_2(PO_4)_3$ nanoparticles anchoring on carbon cloth as a cathode material for sodium-ion batteries have prepared by feasible synthetic method. Two characteristic peaks at 1353 and 1595 cm^{-1} are obtained through Raman spectroscopy. The flexible NVP@NC electrode delivers a higher capacity of 117 mA h g^{-1} than NVP@C at a low rate of 1 C. At a current density of 50 C, the discharge capacity enlarges for NVP@NC electrode as 80.7 mA h g^{-1}. The specific capacity of NVP@NC is 112.3, 105.3, 98.8, 89 and 63 mA h g^{-1} at the rate of 1 C, 2 C, 5 C, 10 C and 20 C respectively. At 1 C, the NVP@NC symmetric complete fuel cell can reach a high energy density of 192 Wh kg^{-1}. This method of preparing NVP@NC shows great potential for constructing other advanced free-standing high-performance electrodes.

[53] Hong-bo Huang *et al.*, (2019) reported double-carbon coated $Na_3V_2(PO_4)_3$ as a superior cathode material for Sodium-ion batteries have prepared by sol-gel method. In this citric acid is used as the chelating agent. XRD patterns shows the well indexed rhombohedral NASICON structure. Two characteristic peaks at 1360 and 1582 cm^{-1} corresponding to the D and G bands are characterized by Raman Spectroscopy. The reduction and oxidation peaks of NVP/C and NVP/C/NC are separated by a voltage of 243 mV and 216 mV, respectively. From the GCD analysis, at current rates of 0.2, 0.5, 1, 2, 5, 10, and 20C, the NVP/C/NC composite displays greater average reversible capacity of 109.8, 107.1, 104.3, 101.5, 97.2, 93.3, and 87.2 mAh g^{-1}, significantly higher than that of NVP/C at the same rate. In this study, it shows that the increased contact area between the active material and the electrolyte, increased the electronic conductivity in the in situ produced nitrogen-doped carbon coating NVP/C/NC composites with high specific capacity, good cycling stability, and superior rate performance.

[54] Haifeng Jiang *et al.*, (2019) have been successfully investigated the selection of graphene dopants for $Na_3V_2(PO_4)_3$ graphene composite as high rate, ultra long-life cathode for sodium-ion batteries. NVP being the most promising cathode materials for sodium-ion batteries. The graphene doped NVP has been synthesized by sol-gel method using Citric acid as the reducing agent to improve electrochemical performance of Sodium-ion batteries. XRD patterns shows the NASICON structure of NVP annealed at 700˚C, 800˚C and 900˚C and the diffraction peaks shows an R-3c space group. At a rate of 0.2C and 0.5C, the discharge specific capacity of NVP-800˚C is 99.06 and 96.91 mAh g^{-1}. When graphene is doped, a higher specific capacity is obtained (113.9 mAh g^{-1} at 0.5C). NVP/N-rGO is being a promising cathode material for energy storage with long-term durability.

[55] Junqi Fang *et al.*, (2019) had prepared the Mn-doped cathode for high-rate ad super stable sodium-ion batteries. Mn-doped $Na_3V_2(PO_4)_3$/C was synthesised by a freeze-drying-assisted thermal treatment method. Citric acid is used as both chelating reagent and a carbon resource. From the XRD analysis, the structure of Mn-doped $Na_3V_2(PO_4)_3$ is rhombohedral. The moderate doping of Mn does not change the structure of $Na_3V_2(PO_4)_3$. The specific discharge capacities were 106.8, 102.7, 97.0, and 90.9 mAh g^{-1} for the current rates of 1, 2, 5, and 10 C. At the rate of 20 C and 30 C, the undoped $Na_3V_2(PO_4)_3$/C electrode exhibits the specific discharge capacity as 67.9 and 60.2 mAh g^{-1}. The freeze-drying method helps to achieve a high surface area to $Na_3V_2(PO_4)_3$ particles with a porous structure. The Mn-doped NVP exhibits 82% capacity retention for up to 10,000 cycles. Therefore, the freeze-drying method is easy and it provides an excellent electrochemical performance towards preparing high performance cathode materials for sodium-ion batteries.

[56] Wenhao Yang *et al.*, (2019) have reported $Na_3V_2(PO_4)_3$/N-doping hard carbon nanocomposites prepared by hydrothermal method. The N-doped NVP exhibit a high initial capacity of 82 mAh g^{-1} at 10 C and with the capacity retention of 84% even after 500 cycles. The best discharge capacity of 117.3 mAh g^{-1} at the rate 0.1 C is exhibited by N-doped $Na_3V_2(PO_4)_3$. Therefore, N-doping can improve the rate performance and the cyclic stability of $Na_3V_2(PO_4)_3$.

[57] Hyeongwoo Kim *et al.*, (2019) have worked on the Polydopamine-derived N-doped carbon-wrapped $Na_3V_2(PO_4)_3$ cathode synthesized by simple sol-gel method. TG-DTA curves obtained in the temperature range of 25-800 ˚C. Initial discharge capacities for NVP and NC@NVP are 104.1 (94.91 $mAhg^{-1}$ at room temperature) and 116.7 $mAhg^{-1}$ (101.0 mAhg1 at

room temperature), respectively. With a high discharge capacity of 107.3 mA hg^{-1}, NC@NVP exhibits outstanding capacity retention at high temperatures, which is 92.0% at the 500th cycle. The polydopamine-derived N-doped carbon-wrapped NVP is expected to be a novel cathode material for sodium-ion batteries. It is also envisaged that the N-doped carbon precursor can be practically used in surface modification for large-scale sodium-ion batteries.

[58] Yanjun Chen *et al.*, (2018) reported F-doped $Na_3V_2(PO_4)_3$/C prepared by the carbon-thermal reduction method. F-doped $Na_3V_2(PO_4)_3$/C of different concentrations are prepared and is used as a cathode material for sodium-ion batteries. XRD patterns shows the structure of rhombohedral NASICON for NVP sample. The concentration of F-0.07-NVP/C composite exhibits the highest conductivity as 4.53 x 10^{-3} S cm^{-1} which is higher than that of Un-doped-NVP/C sample (8.32 x 10^{-4} S cm^{-1}). At the rate of 10, 20, 50, 70, 120, 200 and 10 mA g^{-1}, the discharge capacities of F-0.07-NVP/C are 109.9, 106.5, 104.2, 103.1, 100.6, 96.9, 107.1 mAh g^{-1}. Therefore, the F-doped composite will be a promising cathode material in Sodium-ion batteries for energy storage and conversion.

[59] Xiaqing Chang *et al.*, (2018) have investigated the graphene-bound $Na_3V_2(PO_4)_3$ film electrode with excellent cycle and rate performance for Na-ion batteries. NVP nanoparticles are synthesized by sol-gel method. A graphene-bound $Na_3V_2(PO_4)_3$ film is prepared by the vacuum co-filtration and by thermal treatment, which is being extensively used as both anode and cathode materials for Sodium-ion batteries. Graphene dopant is used because of its high conductivity, thermal stability, and to improve the energy storage in devices. XRD pattern shows the crystal structure of NVP as rhombohedral unit cell with R-3c space group. The initial capacity of the graphene-bound NVP cathode is 114.6 mAh g^{-1}. At the rate of 1C, the initial capacity of the NVP cathode is 65.9 mAh g^{-1}. At the rate of 2C, 5C and 10C, the capacity of the graphene bound NVP cathode is 112, 109.9 and 105.8 mAh g^{-1}. It still maintains a capacity of 89.7 mAh g^{-1} even at a high rate of current density 30 C. The PVDF-bound anode exhibits a poor electrochemical performance which delivers an average capacity of 15 mAh g^{-1} at a current density of 50 mA g^{-1}. But, in the case of the graphene-bound NVP anode exhibits the capacities of about 97.9, 56.8 and 42.3 mAh g^{-1} at current densities of 50 mA g^{-1}, 500 mA g^{-1} and 2 A g^{-1}. In sodium ion batteries, the graphene-bound NVP film electrode is regarded as a promising cathode and anode candidate due to its high active material content.

[60] Qing Zhu *et al.*, (2018) have successfully studied the electrochemical performance of $Na_3V_2(PO_4)_3$/C cathode material for sodium-ion batteries by K-Ca co-doping. NVP cathode

material are synthesized by sol-gel method followed by the freeze-drying process and high temperature calcination processes. Citric acid is used as both chelating agent and reducing agent. The structure of K-Ca co-doped $Na_3V_2(PO_4)_3$ is rhombohedral. Flame atomic absorption spectrophotometry determined the compositional data of pristine and co-doped $Na_3V_2(PO_4)_3$ samples. The optimal doping samples of NVP/C shows the reversible capacities of 110.2, 92.7 and 83.6 mAh g^{-1} at the current densities of 0.1, 1 and 10 C. The effect of co-doping of K^+ and Ca^{2+} shows improvement in the electrochemical performance of NVP/C cathode which shows that co-doped K-Ca-NVP/C is a promising cathode material for Sodium-ion batteries.

[61] Wei Zheng *et al.*, (2018) reported Ni^{2+} doped $Na_3V_2(PO_4)_3$ have prepared by spray drying-assisted method. Ni doped $Na_3V_2(PO_4)_3$ used as a cathode material in sodium-ion batteries. The electrical conductivity of NVP/C, NVP/C-Ni-1, NVP/C-Ni-2, NVP/C-Ni-3 and NVP/C-Ni-4 cathode materials is 7.21 x 10^{-2}, 8.11 x 10^{-2}, 8.72 x 10^{-2}, 9.13 x 10^{-2} and 9.34 x 10^{-2} S cm^{-1}. At a rate of 5 C, the Ni-doped $Na_3V_2(PO_4)_3$ exhibits a discharge capacity of 104.5 mAh g^{-1}. Even after 1000 cycles, an excellent capacity retention of 95.4 % is maintained at 5C.

[62] Lina Zhao *et al.*, (2018) successfully investigated the superior high-rate and ultralong lifespan $Na_3V_2(PO_4)_3$ cathode by enhancing the conductivity in Sodium-ion batteries. Ti-doped $Na_3V_2(PO_4)_3$ have prepared by the solvothermal-assistant reaction. Raman spectrum shows peaks at 1360 and 1584 cm^{-1} for D and G bands. The capacity of Ti-doped $Na_3V_2(PO_4)_3$ is 116.6 mAh g^{-1} at 1 C which is approximately equal to its theoretical value. The electrode still delivered 93.4 mAh g^{-1} at an ultrafast current density of 400 C. NVP based cathode materials are been a best electrode and shows a better electrochemical performance in Sodium-ion batteries.

[63] Qiong Zheng *et al.*, (2017) reported $Na_3V_2(PO_4)_3$ through Ce/V substitution as a cathode material prepared by Sol-gel method. By Ce doping in NVP sample, it shows the highest electrochemical performance. When Ce doping takes place, the initial discharge capacity seems to be increased at first and then decreases related to the value of 111 mAh g^{-1}, 112 mAh g^{-1}, 118 mAh g^{-1}, 114 mAh g^{-1} and 109 mAh g^{-1} at the rate of 0.2 C for the $Na_2V_{2-x}(PO_4)_3$/C samples with the concentration range of 0, 0.02, 0.04, 0.06 and 0.1 at the rate of 1C, 2C, 5C, 10C, 20C and 40C. The 2 mol% Ce-doping sample produced an initial discharge capacity of 118 mAh g^{-1}, which is extremely close to the theoretical specific capacity, at low rate of 0.2C. The discharge capacity is still seeming to be greater than 100 mAh g^{-1} even at 40C. The improved bulk phase feature brought on by metallic ion doping while omitting the impact of the carbon

covering using EIS measurement. This study gives a big promotion to industrial applications of NVP cathode for high performance sodium-ion batteries.

[64] Atsushi Inoishi *et al.*, (2017) studied the improvement in the energy density of $Na_3V_2(PO_4)_3$ by Mg-substitution. Mg substituted $Na_3V_2(PO_4)_3$ was synthesised by the sol-gel method. The structure of $Na_3V_2(PO_4)_3$ was rhombohedral and is determined by the X-ray diffraction (XRD). The reversible capacity of Mg-substituted $Na_3V_2(PO_4)_3$ is higher than that of the theoretical capacity of the undoped $Na_3V_2(PO_4)_3$ (117.6 mAh g^{-1}). Therefore, Mg-substituted $Na_3V_2(PO_4)_3$ is said to be one of the promising cathode materials in sodium-ion batteries.

[65] Huaixin Liu *et al.*, (2017) evaluated the behaviour of N-doped graphene decorated $Na_3V_2(PO_4)_3$/C composite synthesized by sol-gel method. XRD pattern and SEM results indicate the NASICON structure $Na_3V_2(PO_4)_3$/C with the particle size of 120 nm. The graphitic structure corresponds to the D-band (1588 cm^{-1}), whereas the structural disorder site is associated to the D-band (1362 cm^{-1}). When the N-graphene sheets were introduced, the surface area of the increases to 27.3 m^2 g^{-1}. The specific capacity is 94.1 mAh g^{-1} at 10 C and it can still retain as 99.6% even after 5 cycles. The highly conducting N-graphene sheets greatly improve the composite's electrochemical performance, which exhibits exceptional high- rate capability and long-cycle stability. Therefore, the $Na_3V_2(PO_4)_3$/C@N-graphene is a promising cathode material to be used in sodium-ion batteries.

[66] Bao Zhang *et al.*, (2017) demonstrated the synthesis and electrochemical performance of Ni-doped $Na_3V_2(PO_4)_3$/C cathode materials for sodium-ion batteries. Simple sol-gel synthesis was used to create the cathode materials NVP/C and Ni doped NVP/C. XRD pattern reveals the monoclinic structure and it was not changed even while Ni-doping. SEM was used to characterize the morphology of the sample and it was found to be rough after Ni-doping. In Raman Spectrum, the lower intensity of the D band at 1348 cm^{-1} and comparison with G band 1593 cm^{-1}. $Na_3V_{1.97}Ni_{0.03}(PO_4)_3$/C exhibited a specific capacity of 98.1 mAh g^{-1} at the rate of 5 C. Therefore, the Ni-doping significantly enhanced rate and cycling performances.

[67] Huang Zhang *et al.*, (2017) have studied the effect of nitrogen doping on the structure of $Na_3V_2(PO_4)_3$ (NC-coated NVP) cathode for sodium-ion batteries. NC-coated NVP was synthesized by solid-state reaction. XRD pattern reveals that the sample is rhombohedral in structure. TEM is used to characterize the morphology and structure of NVP. The structural

analysis of the carbon coatings was done by the Raman spectroscopy. In Raman spectrum, the peaks are present at 1357 cm^{-1} and 1593 cm^{-1} corresponds to D and G bands. The NVP materials can have high energy and power efficiency and thanks to the N-doping of the carbon, which results in greatly reduced electrode polarization and excellent cycle stability at high rate.

[68] Huang Zhang *et al.*, (2017) have successfully investigated the excellent cycling stability and superior rate capability of $Na_3V_2(PO_4)_3$ (NVP-NC) cathodes by nitrogen-doped carbon for Sodium ion batteries. N-doped $Na_3V_2(PO_4)_3$ was synthesized by one-step solid-state reaction. X-ray diffraction (XRD) and Scanning Electron Microscopy (SEM) were used to characterize the Structure and Morphology of the synthesized $Na_3V_2(PO_4)_3$. XRD pattern shows the rhombohedral structure for NVP-NC. At 0.1 C, 0.5 C, 1 C, 5 C, 10 C, and 20 C, the NVP/N-CNT electrode offers a capacity of 178 mAh g^{-1}, 166 mAh g^{-1}, 161 mAh g^{-1}, 148 mAh g^{-1}, 141 mAh g^{-1}, and 128 mAh g^{-1}. Even at 5 C, it delivers a high capacity of 147 mAh g^{-1}. NVP materials are made possible by the N-doped carbon coating, which makes both high-performance positive and negative electrodes with superior rate capability and cycling stability.

[69] Qing Qiu *et al.*, (2021) reported $Na_3V_2(PO_4)_3$ cathode material have prepared by sol-gel process followed by solid-state reaction. The theoretical capacity of NVP 400 Wh kg^{-1}. XRD pattern shows rhombohedral structure for NVP. The objective of this research is to enable a fourth Na+ intercalation during discharge, increasing the theoretical specific capacity to about 494 Wh kg^{-1}.

[70] Claudio Gerbaldi *et al.*, (2020) reported Nano fibre $Na_3V_2(PO_4)_3$ had prepared through co-precipitation method and it is used as a Self-Standing Cathode material for Sodium-ion batteries. The advantages of the electrospinning technique is to provide a flexibility to tune some nanofibers at certain degrees such as the diameter of the fibres and thickness. The theoretical capacity of Na-half cells is 220 μ Ah cm^{-2} whereas the obtained total capacity is 265 μ Ah cm^{-2}. The total capacity after 70 cycles remains to be 200 μ Ah cm^{-2} which is lesser than other NVP-based electrode materials. The high C-rate capability and the good cycling of the NVP-CNF's composite have performed for more than 200 cycles, without major degradation of performances was confirmed through the electrochemical testing. These materials are self-supported, long-term performing NIB electrodes and are used for the future generation electrodes in Na-ion batteries.

From the review of literature, it is understood well that $NaVOPO_4$ is more sought compound than $Na_3V_2(PO_4)_3$ with fluorination or carbonation due to the simple monoclinic structure that favors the intercalation process more. Most of the literature, to the best knowledge of the author, is on $Na_3V_2(PO_4)_3$ and very few reports are available on $NaVOPO_4$. Hence, this study focuses on achieving single phase monoclinic structure of $NaVOPO_4$ and influence of doping in it.

MATERIALS AND METHODS

CHAPTER III

MATERIALS AND METHODS

3.1. Introduction

This chapter discusses the materials, preparation methods and characterization techniques of Sodium Vanadium (IV) phosphate or Sodium vanadato (IV) phosphate ($NaVOPO_4$). Copper, Zirconium, Lanthanum and Titanium doped Sodium Vanadium phosphate ($NaVOPO_4$) have also been studied. Sodium Vanadium Phosphate ($NaVOPO_4$) and doped $NaVOPO_4$ is synthesized by using the sol-gel technique. The properties of the materials are characterized by some experimental techniques.

They are:

- **X-ray Diffraction (XRD)**

  The basic characterization of material properties such as crystal structure, crystallite size and strain are carried out by X-ray Diffraction (XRD).

- **Cyclic Voltammetry**

  Cyclic Voltammetry is an electrochemical method used to measure the current response of a redox active solution to a linearly cycled potential sweep.

3.2. Preparation Methods

There are several techniques which are employed to synthesize the nanoparticles. Some of the synthesis techniques processes are;

- Co-Precipitation Process
- Hydrothermal Method
- **Sol-Gel Process**
- Solid-State Reaction
- Carbothermal Reduction Method
- Solvothermal Reaction
- Reflux Method

3.2.1. Sol-gel method

The sol-gel method is a chemical (wet chemical) method for creating different nanostructures, particularly metal oxide nanoparticles. In this method, the molecular precursor is dissolved in water or alcohol and hydrolyzed, or heated and stirred, to convert into a gel. The Sol-gel process is performed at low temperature and in the liquid state. The Sol-gel process is carried out for the preparation of Sodium Vanadium phosphate ($NaVOPO_4$).

3.2.1.1 Advantages of Sol-gel method

1. Simplicity of the process
2. Preparation of high purity products
3. Synthesis of uniform compounds in the form of composite oxides
4. High chemical reactivity of precursors due to process in solution phase.
5. Production of porous and rich materials with organic and polymeric compounds. **[71]**

3.3. Synthesis of Sodium Vanadium (IV) phosphate and doped samples

Sodium Vanadium phosphate (NVP) is prepared by Sol-gel process and the same procedure is carried out for the Cu, Zr, La, Ti doped samples. For the preparation of Sodium Vanadium phosphate ($NaVOPO_4$), Sodium Carbonate (Na_2CO_3) and Ammonium Metavanadate (NH_4VO_3) are used as the starting materials.

The chemical reaction involved in the preparation of Sodium Vanadium (IV) Phosphate are as follows:

$$9Na_2CO_3 + 18NH_4VO_3 + 18NH_4H_2PO_4 + C_6H_8O_7.\,H_2O \rightarrow 18NaVOPO_4 + 36NH_3 + 15\,CO_2 + 41\,H_2O$$

3.3.1. Materials Used

1. Sodium carbonate (Na_2CO_3)
2. Ammonium metavanadate (NH_4VO_3)
3. Ammonium dihydrogen phosphate ($NH_4H_2PO_4$)
4. Citric acid monohydrate ($C_6H_8O_7.\,H_2O$)
5. Copper (II) nitrate Trihydrate ($Cu(NO_3).\,3H_2O$)
6. Zirconyl nitrate Hydrate ($H_2N_4O_{13}Zr$)
7. Lanthanum nitrate hexahydrate ($La(NO_3)_3.\,6H_2O$)

8. Titanium (IV) butoxide ($Ti(C_4H_9O)_4$
9. Distilled Water

3.3.2. Preparation of Pure Sodium Vanadium phosphate (NVP-pure)

Sodium Vanadium phosphate ($NaVOPO_4$) is synthesized by the sol-gel method.

The preparation method involves the following steps which is shown in the **Figure. 3.1.**

Step 1: A measure of 0.03 M of Citric acid monohydrate ($C_6H_8O_7. H_2O$) is dissolved in 50 ml of distilled water and is stirred for 30 min at 80 ˚C.

Step 2: Then, 0.01M of Sodium Carbonate (Na_2CO_3), 0.02 M Ammonium Metavanadate (NH_4VO_3) and 0.02 M Ammonium Dihydrogen Phosphate ($NH_4H_2PO_4$) are added to the citric acid monohydrate solution and is stirred for 4 hours at 80 ˚C.

Step 3: After 4 hours of stirring, the prepared solution is heated at 90 ˚C to form sol-gel intermediates.

Step 4: The gel is further kept in hot air oven to form a dry powder.

Step 5: The resultant powder sample is transferred to a crucible and kept in furnace for further calcination at 500 ˚C for 5 hours.

Step 6: The obtained powder sample is ground finely with a mortar and pestle to form a final product i.e., olive green in color.

3.3.3. Preparation of Copper, Zirconium, Lanthanum, Titanium doped NVP

- In the case of doped samples, 0.02 M of Copper (II) nitrate Trihydrate ($Cu(NO_3). 3H_2O$), Zirconyl nitrate Hydrate ($H_2N_4O_{13}Zr$), Lanthanum nitrate hexahydrate ($La(NO_3)_3. 6H_2O$) and Titanium (IV) butoxide in 20 ml are added along with the materials said in step 2 and the same procedure is repeated for each dopant.

- The doping of element was done in the B-site of pure NVP where it can be represented as $NaV_{(1-x)}(A)_xPO_4$.

  Where, A = Cu, Zr, La and Ti

  x = 0.02

- Therefore, the samples are represented as $NaV_{0.18}Cu_{0.02}PO_4$, $NaV_{0.18}Zr_{0.02}PO_4$, $NaV_{0.18}La_{0.02}PO_4$ and $NaV_{0.18}Ti_{0.02}PO_4$, which can be named as NVP-Cu, NVP-Zr, NVP-La and NVP-Ti.

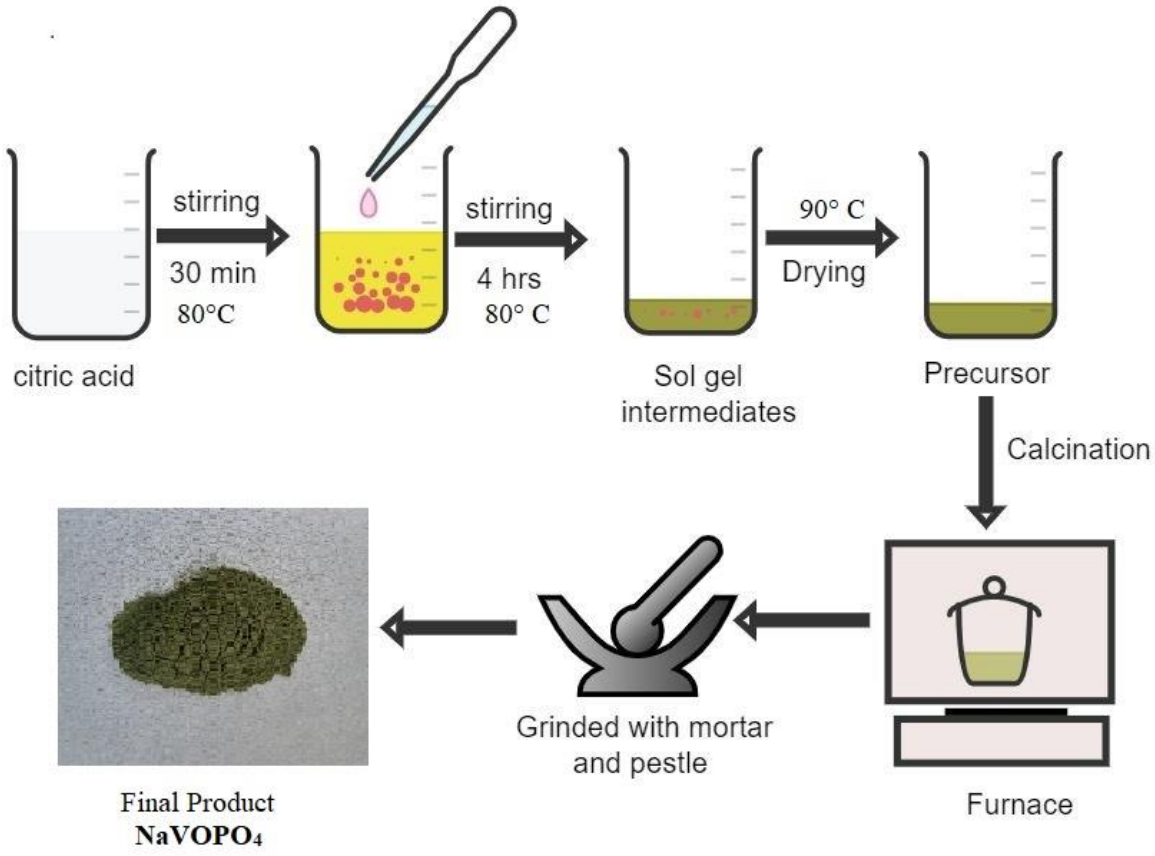

Figure 3.1. Preparation of $NaVOPO_4$

Copper, Zirconium, Lanthanum and Titanium substituted Sodium Vanadium (IV) phosphate is prepared by the above Sol-gel method and the final samples are used for further characterization purpose.

3.4. STRUCTURAL CHARACTERIZATION

3.4.1. X-ray diffraction

X-rays are electromagnetic radiation with very short wavelengths and high energy.

X-ray Diffraction (XRD) is a versatile, non-destructive technique that give the detailed information about the chemical composition and crystallographic structure of materials.

3.4.1.1. Powder X-ray diffraction

Powder X-ray diffraction is used to characterize crystallographic structure, grain size, and preferred orientation in polycrystalline or powder solid samples. This method is preferable method for analysis for characterization of unknown crystalline materials.

3.4.1.2. Crystal structure and unit cell

- Crystallography diffraction data provides the information on the structure of crystalline solids.
- Atoms in a crystal are arranged in periodic configurations called crystal structures.
- Lattices (an infinite array of points in space) are used to define structures.
- The smallest repeating structure in a crystalline material's lattice is referred to as a unit cell.
- This gives rise to the constructive interference which is defined by Bragg's Law. **[72]**

3.4.1.3. Principle of X-ray diffraction

- Max von Laue discovered in 1912 that crystalline materials which behaves for X-ray wavelengths as three-dimensional diffraction gratings identical to the spacing planes in a crystal lattice.
- X-ray diffraction is a widely used method for examining crystal structures and atomic distances.
- XRD works on the principle of Bragg's equation which can be explained in terms of reflection of collimated X-ray beam incidence on a crystal plane of the sample to be characterized.

3.4.1.4. Bragg's law

- The principle of X-ray diffraction is constructive interference of monochromatic X-rays and a crystalline sample. Bragg provided an alternative description and measurement for diffraction of monochromatic x-ray from single crystal after Laue discovery of the X-ray diffraction. **[73]**
- The Bragg's analysis made the assumption that crystals are made up of layers or that atomic planes (also known as lattice planes, or hkl) are arranged in layers with a spacing distance, d, and create reflection when incident light or x-rays impinge on those planes of atoms. Figure 3.2.a.

- At the lattice plane, the incident beam and the corresponding diffracted beam make an equal angle.

When constructive interference occurs, the Pythagorean theorem and the Bragg's diffraction condition are satisfied. Figure 3.2.b

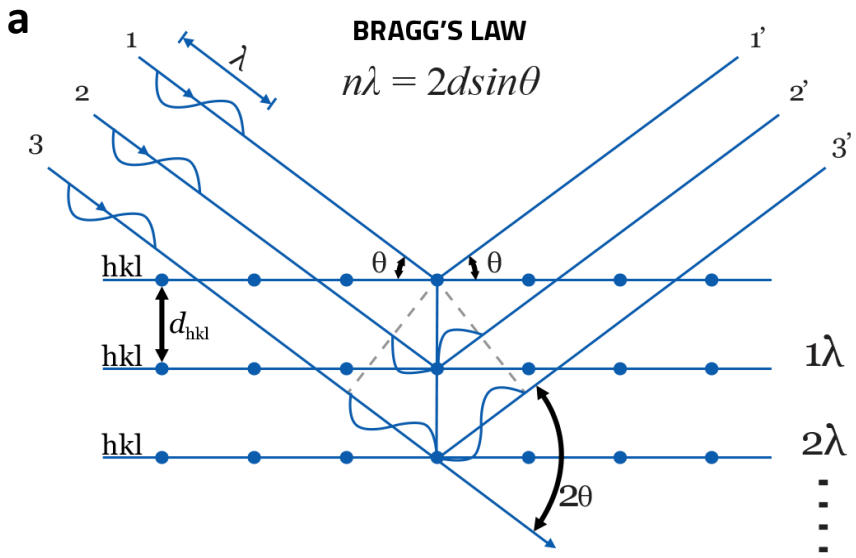

Figure. 3.2.a Schematic representation of X-ray diffraction pattern

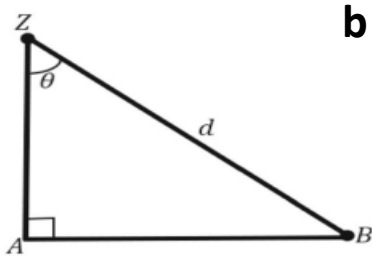

Figure 3.2.b Pythagoras theorem

According to the Bragg's law constructive interference occurs;

If, AB+BC =n λ

From the x-ray diffraction pattern, AB=BC,

n λ = 2AB

By Pythagoras theorem;

$$\text{Sin } \theta = \frac{AB}{d}$$

$$AB = d \sin \theta$$

$$N \lambda = 2d \sin \theta$$

where,

λ = x-ray wavelength

n = order of reflection

d = spacing distance

θ = angle of diffraction.

Since, the order of diffraction (reflection) from set of lattice planes (hkl) with interplanar spacing d_{hkl}.

$$d = d_{hkl}/n$$

Then, the equation $n \lambda = 2d\sin \theta$ can be written by substituting into

$$\lambda = 2d_{hkl}\text{sion } \theta_{hkl}$$

Therefore, the Bragg's law in vector notation is expressed;

$$\frac{(S-S0)}{\lambda} = d^*_{hkl} = ha_1 + ka_2 + la_3 \text{ (Figure 3.2.c)}$$

Where, S= unit vector along diffracted beam direction.

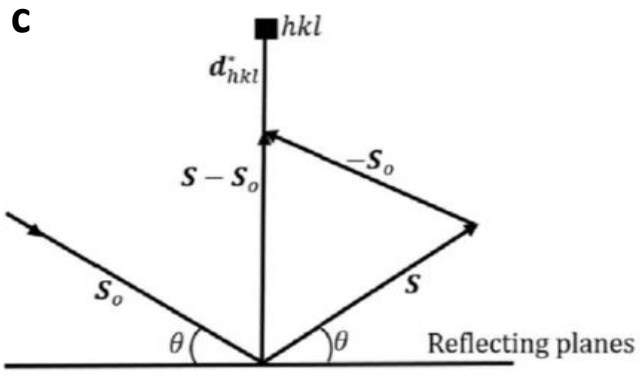

Figure 3.2.c. Diagrammatic representation of Bragg's law in vector notation

3.4.1.5. Scherrer's equation

Scherrer's equation is used to calculate the nano-crystalline size accurately using XRD. This equation is introduced by Scherrer in 1918 for calculating the crystalline size of the materials and the equation

$$D = \frac{k\ \lambda}{\cos\theta}$$

where,

D is the crystallite size (nm),

λ is the wavelength of x-ray beam (nm),

θ is the diffraction angle (degrees)

β (in radian) is the peak width (full width at half maximum),

k is the Scherrer's constant (0.89)

'k' value depends upon the width of the diffraction peak, the crystallite size distribution, the crystalline shape, and the diffraction line index. k value varies from 0.62 and 2.08, while in the absence of information on crystalline shape, it is used as 0.89. The diffraction peak's breadth in Scherrer's equation is the full width at half of the diffraction peak height. **[74]**

3.4.1.6. Instrumentation

X-ray Diffractometer consists of Collimator, X-ray tube, Detector and Sample holder. Figure 3.3.

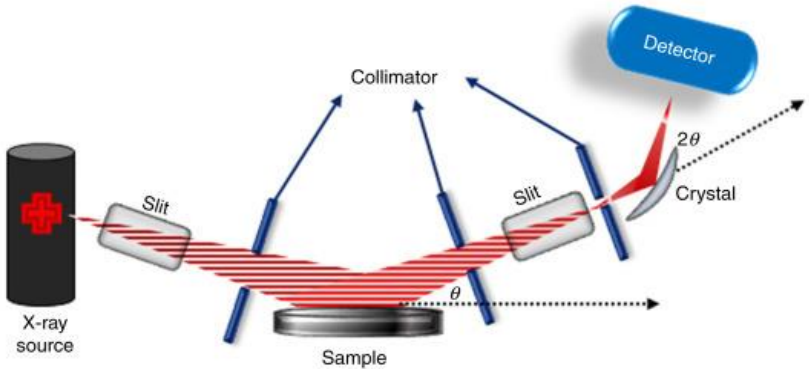

Figure 3.3. Schematic representation of XRD

Collimator:

X-rays are generated by the target material when allowed to pass through a collimator. It consists of two sets of closely packed metal plates separated by a small gap. Collimator absorbs all the X-rays, but the narrow beam that passes between the gaps is not absorbed. **[75]**

Crystal Monochromators

These are made up of a suitable crystalline material positioned in the x-ray beam so that the angle of reflecting planes satisfied the Bragg's equation for the required wavelength, and the beam is split up into component wavelengths.

Detectors:

Detectors use different types of methods to detect X-rays. They are:

Photographic Methods

$$D = \log I_0 / I$$

where,

I_0 = Incident intensities.

I = Transmitted intensities.

D = Total energy that causes the blackening of the film.

Counter Methods

It is divided as follows:

(i) Geiger-Muller Tube Counter
(ii) Proportional Counter
(iii) Scintillation Detectors
(iv) Solid State Semiconductor Detectors
(v) Semiconductor Detectors.

3.4.1.7. Advantages and applications of XRD

- XRD is a non-destructive technique
- Identify crystalline phases and orientation
- Determine the structural properties
  - Lattice parameters
  - Strain
  - Grain Size
  - Epitaxy
  - Phase Composition
  - Preferred orientation
- Measure thickness of thin films and multi-layers
- Determine atomic arrangement

3.4.1.8. Disadvantages of XRD

- XRD analysis requires access to standard reference data. Preparation of samples oftern requires grinding them down to a powder. If the crystal sample is non-isometric, then the indexing of patterns can be complex when determining unit cells.
- XRD also have size limitations. It is much more accurate for measuring large crystalline structures than the small ones. Small structures that are present only in trace amounts will often go undetected by XRD readings.

3.5. CYCLIC VOLTAMMETRY

Cyclic Voltammetry is an electrochemical method used to measure the current response of a redox active solution to a linearly cycled potential sweep.

It is used to study the electrochemical behaviour of species diffusion to an electrode surface, interfacial phenomena at an electrode surface.

The diffusion and migration of ions carries this current through the solution.

3.5.1. Principle

Cyclic voltammetry is a method in which the potential applied to an electrochemical cell is scanned. **[76]**

The resulting cell output is plotted as graph against output and potential. Figure 3.4.

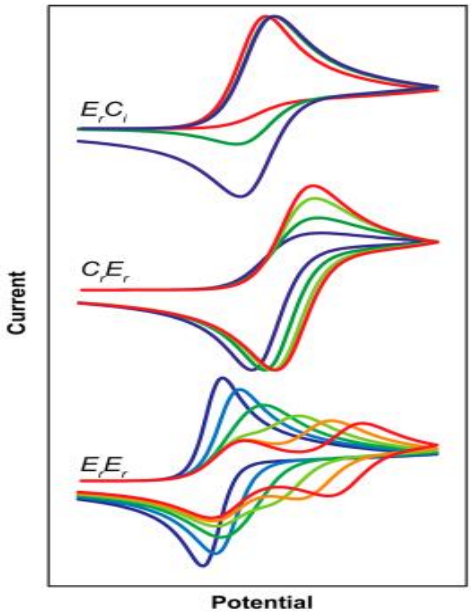

Figure 3.4. Graph for Cyclic Voltammetry

3.5.2. Instrumentation

A Cyclic Voltammetry consists of an electrolysis cell, potentiostat, a current-to-voltage converter, and a data acquisition system. The electrolysis cell consists of a working electrode, counter electrode, reference electrode and electrolytic solution. **[77]** Figure 3.5.

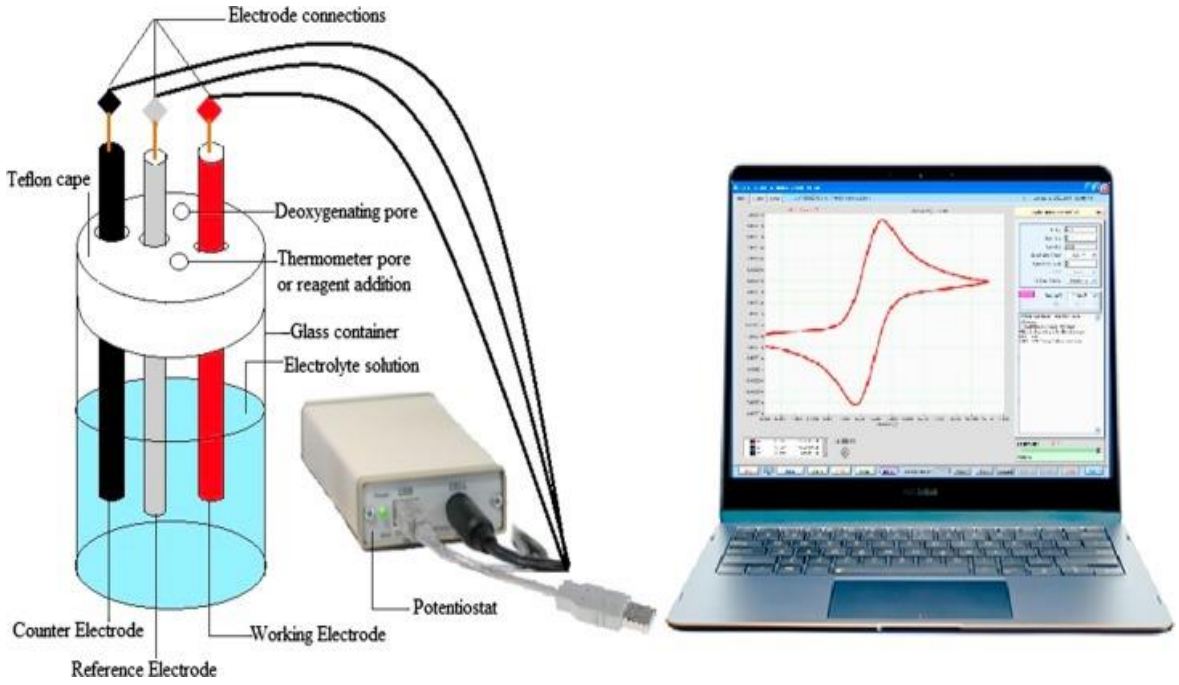

Figure 3.5. Schematic representation of Cyclic Voltammetry

- **Working electrode (WE)**

The working electrode carries out the electrochemical event of interest. A potentionstat is used to control the applied potential of the working electrode as a function of the reference electrode potential. The working electrode's composition in the potential range of interest, which is redox inert, is its most crucial feature.

- **Reference electrode (RE)**

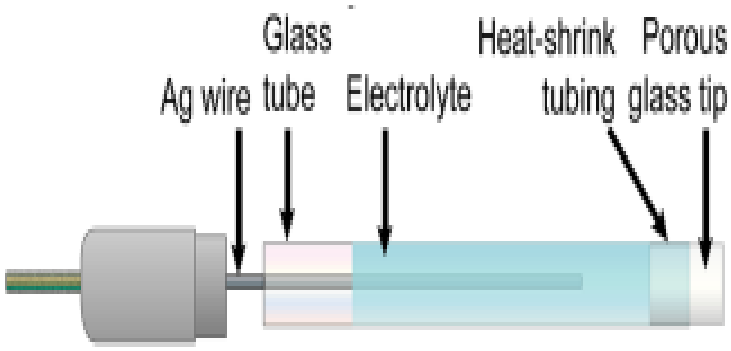

Figure 3.6. Schematic representation of Reference Electrode

The reference electrode is a well-defined and stable equilibrium potential. When measuring the potential of other electrodes in an electrochemical cell, it serves as a reference point. Some common reference electrodes used in an aqueous media includes the saturated calomel electrode (SCE), standard hydrogen electrode (SHE) and AgCl/Ag electrode.

- **Counter electrode (CE)**

When a potential is applied to the working electrode such that reduction (or oxidation) of the analyte can occur, current begins to flow. The purpose of the counter electrode is to complete the electrical circuit. Current is recorded as electrons flow between the WE and CE. To ensure that the kinetics of the reaction occurring at the counter electrode do not inhibit those occurring at the working electrode, the surface area of the counter electrode is greater than the surface area of the working electrode.

3.5.3. Applications

- Cyclic voltammogram is employed in organic and inorganic chemistry.
- The good temporal and chemical resolution of such in-vivo cyclic voltammetric experiment offers improved understanding of the chemistry of the brain.

- Industrial corrosion processes are being monitored using CV technique.
- Cyclic Voltammetric detectors have large applications in chromatography. **[78]**

3.5.4. Advantages

- The technique is prominent with its advantages of simplicity, sensitivity, speed and low costs which results in a wide range of applications.

3.5.5. Limitations

- There is a background charging current throughout the experiment.
- This causes a restriction in the detection limit. In addition, the ratio of the peak faradic current to the charging current decreases with increasing v as i_p is proportional to $v^{1/2}u^{1/2}$.

RESULTS AND DISCUSSION

CHAPTER IV

RESULT AND DISCUSSIONS

4.1. Introduction

This chapter deals with the analysis of the synthesized Sodium Vanadium phosphate NVP-pure, NVP doped with di valent elements Cu^{2+} (NVP-Cu), Zr^{2+} (NVP-Zr) and tri valent elements La^{3+} (NVP-La), Ti^{3+} (NVP-Ti) synthesized using the sol-gel method. The structural and electrochemical performance of the prepared samples are characterized using X-Ray Diffraction (XRD) and Cyclic Voltammetry (CV) which are discussed in this chapter.

4.2. Structural Characterization

4.2.1. X-Ray Diffraction (XRD) Analysis

4.2.1.1. XRD Analysis for pure $NaVOPO_4$ (NVP-pure)

The structural analysis is carried out by Bruker AXSD2 Phaser at room temperature to determine the phase formation. The XRD pattern of pure $NaVOPO_4$ (NVP-pure) is shown in Figure 4.1. A pure phase of NVP has been obtained and it is indexed with the **JCPDS Card No. 76-0417. [79]**

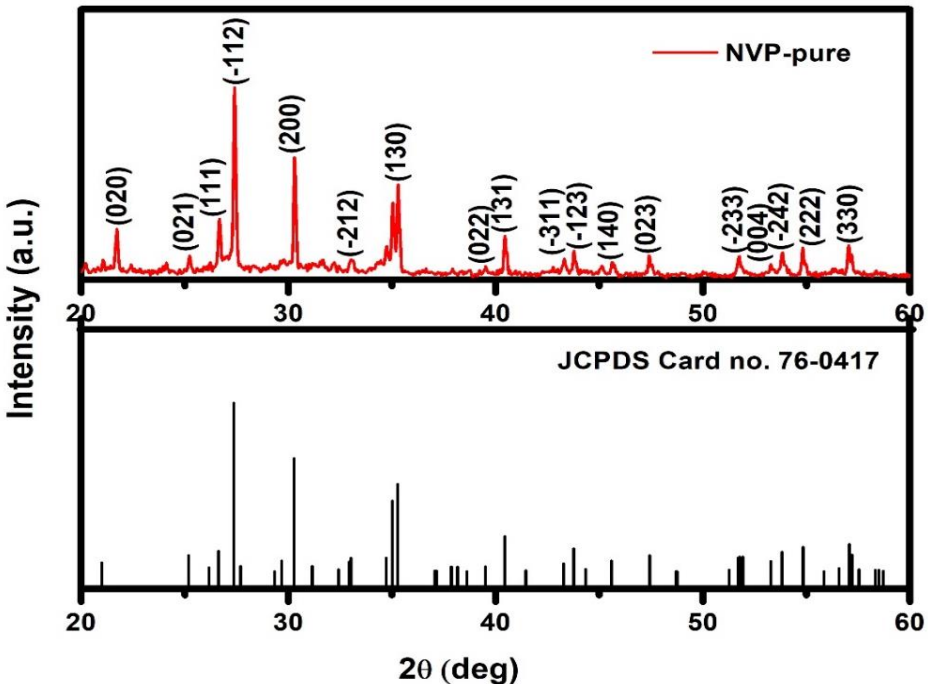

Figure 4.1. XRD pattern of pure phase of $NaVOPO_4$ (NVP-pure)

The XRD pattern are in good agreement with $NaVOPO_4$ with a monoclinic crystal structure. The XRD peaks well agree with the standard XRD pattern of $NaVOPO_4$ (JCPDS card no. 76-0417). The major diffraction peaks are observed at 2θ = 27.3˚, 30.2˚, 18.3˚ and their corresponding miller planes are (-112), (200) and (110). The miller planes of the other peaks are (130), (022), (-111), (131), (330), (222), (-242), (-123), (111), (-102), (-233), (140), (004), (023), (-212), (031) and (004). The diffraction peaks are assigned to the monoclinic structure of space group $P2_1/c$ with lattice parameters a = 6.524 Å, b = 8.455 Å and c = 7.119 Å and volume 355.05 $Å^3$. **[80], [81].**

The crystallite size, D, can be estimated from the peak width using Scherrer's formula,

$$\mathbf{D = \frac{k\lambda}{\beta cos\theta}\ (nm)} \quad \text{-------- (1)}$$

were,

D is the crystallite size (nm),

λ is the X-ray wavelength (0.154 nm),

β is the full-width half maximum (FWHM) of a diffraction peak (rad)

k is the Scherrer's constant (0.89)

The strain can be calculated from the formula,

$$\mathbf{\varepsilon = \frac{\beta}{4tan\theta}} \quad \text{-------- (2)}$$

Table 4.1. Parameters obtained from the major peak of the XRD pattern of NVP-Pure

Sample name	2θ (deg)	β (FWHM)	Crystallite size (nm)	Strain
NVP-Pure	27.3	0.1340	61.18	0.064

The crystallite size and the strain of pure phase of $NaVOPO_4$ (NVP-pure) are calculated using the maximum intense peak observed at 2θ = 27.3˚ with hkl plane (-112) which is shown in the Table 4.1.

4.2.1.2. XRD Analysis for Cu-doped $NaVOPO_4$ (NVP-Cu)

The XRD diffraction peak of Cu-doped $NaVOPO_4$ is well agreed with the standard XRD pattern of pure $NaVOPO_4$ (JCPDS Card no. 76-0417). The major diffraction is observed at $2\theta = 27.3^{\circ}$ and the corresponding miller planes is (-112) which is same as the pure phase of $NaVOPO_4$. The other peaks observed from the XRD diffraction pattern are also in good agreement with the JCPDS Card No. 76-0417. The corresponding miller planes for the peaks are (020), (021), (111), (200), (-212), (031), (022), (130), (102), (112), (131), (-123), (140), (023), (-313), (202), (-233), (004), (222) and (330) respectively. The XRD pattern of Cu-doped $NaVOPO_4$ (NVP-Cu) is shown in Figure 4.2.

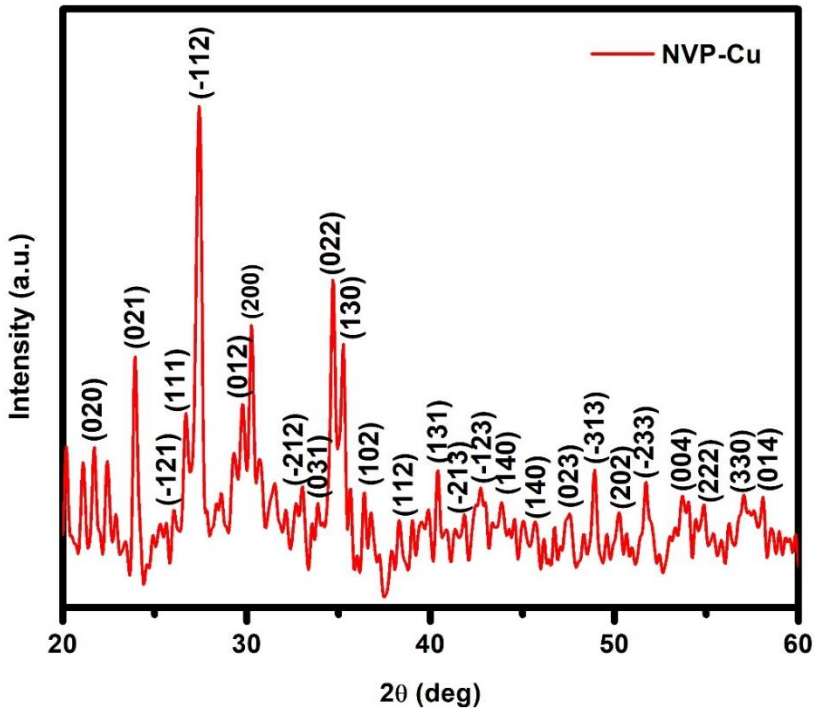

Figure 4.2. XRD pattern of NVP-Cu

Table 4.2. Parameters obtained from the major peak of the XRD pattern of NVP-Cu

Sample name	2θ (deg)	FWHM β (deg)	Crystallite size (nm)	Strain
NVP-Cu	27.3	0.4126	19.83	0.19

The crystallite size and strain of the Cu-doped $NaVOPO_4$ (NVP-Cu) are calculated using the maximum intense peak observed at $2\theta = 27.3^{\circ}$ and is shown in the Table 4.2.

A lower value of crystallite size is observed for the Cu-doped NVP where the di-valent dopant atom of Cu^{2+} could eventually decrease the size of the crystal upon doping with pure NVP. This is an added advantage for the electrochemical cycling for the doped sample.

4.2.1.3. XRD Analysis for Zr-doped $NaVOPO_4$ (NVP-Zr)

The XRD pattern of Zr-doped $NaVOPO_4$ (NVP-Zr) is shown in Figure 4.3. XRD pattern of NVP-Zr are in agreement with the pure phase of $NaVOPO_4$ with a monoclinic crystal structure. For the pure phase of $NaVOPO_4$, the major peak is observed at $2\theta = 27.3^{\circ}$ but, the major diffraction peak for Zr-doped $NaVOPO_4$ (NVP-Zr) is observed at $2\theta = 30.6^{\circ}$ and the corresponding miller plane for Zr-doped $NaVOPO_4$ is (200) indicating different orientation of the crystallites due to doping.

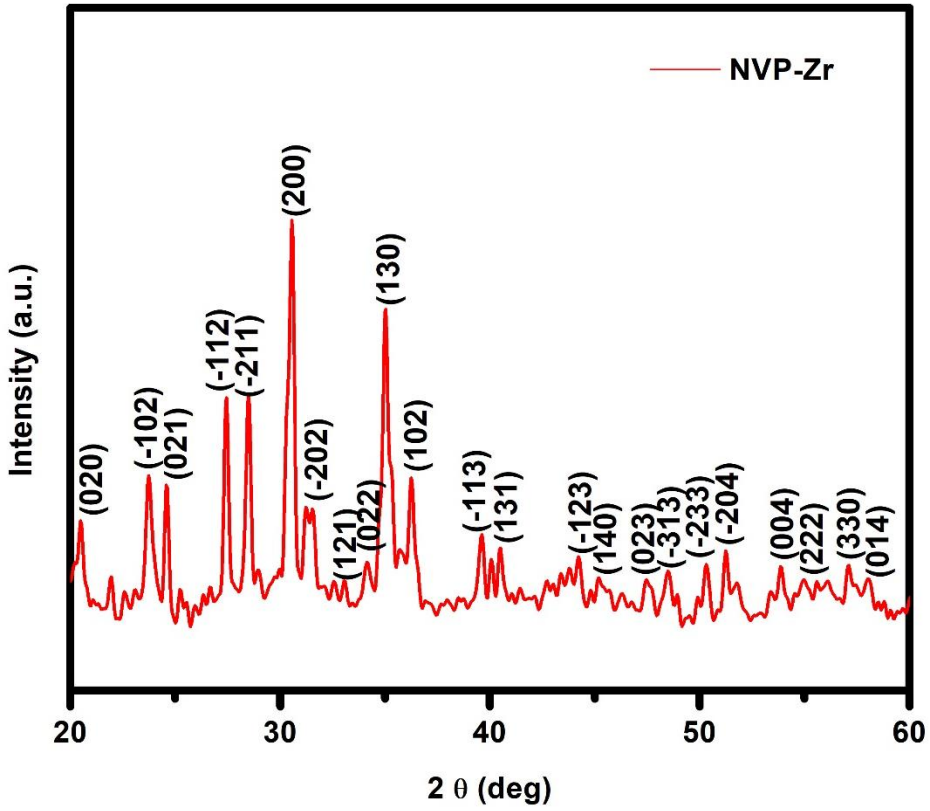

Figure 4.3. XRD pattern of NVP-Zr

The intensity of the major peak alone changes from the pure phase of $NaVOPO_4$. The other peaks of NVP-Zr are matched with the JCPDS Card No. 76-0417.

Table 4.3. Parameters obtained from the major peak of the XRD pattern of NVP-Zr

Sample name	2θ (deg)	FWHM β (deg)	Crystallite size (nm)	Strain
NVP-Zr	30.6	0.1933	42.46	0.081

The crystallite size and strain for Zr-doped $NaVOPO_4$ (NVP-Zr) are calculated using the maximum intense peak observed at 2θ = 30.6˚. The di valent dopant Zr^{2+} shows lower crystallite size than the pure NVP which is shown **Table 4.3.** Lower crystallite size can also be a reason for (200) orientation.

4.2.1.4. XRD Analysis for La-doped $NaVOPO_4$ (NVP-La)

The XRD pattern of La-doped $NaVOPO_4$ (NVP-La) is shown in Figure 4.4. XRD pattern of NVP-La are in good agreement with the pure phase of $NaVOPO_4$ with a monoclinic crystal structure. In the case of La-doped $NaVOPO_4$ (NVP-La), the first major diffraction peak observed from the XRD pattern is 27.4˚ and it exactly matched with the major peak of pure $NaVOPO_4$. The corresponding miller plane for the first major peak of La-doped $NaVOPO_4$ (NVP-La) is (-112).

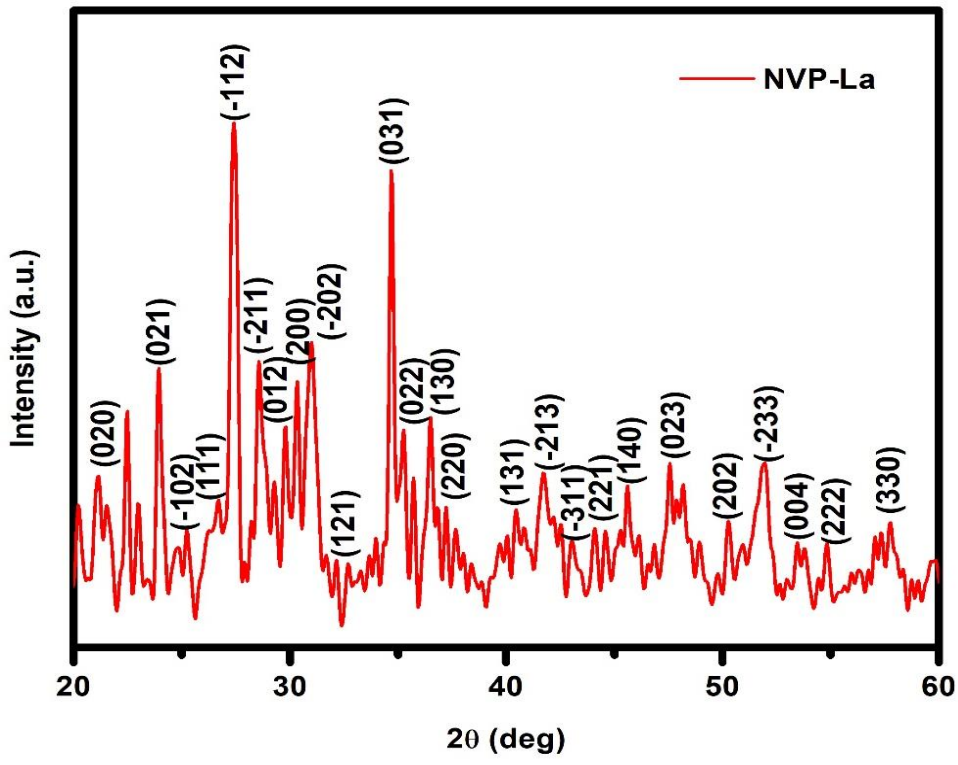

Figure 4.4. XRD pattern of (NVP-La)

The other peaks are also matched with the JCPDS Card No.76-0417 but the intensity of the diffraction peak alone changes. Therefore, when La is doped in NVP lattice, no much changes in the crystal structure are observed.

Table 4.4. Parameters obtained from the major peak of the XRD pattern of NVP-La

Sample name	2θ (deg)	FWHM β (deg)	Crystallite size (nm)	Strain
NVP-La	27.4˚	0.1445	56.73	0.069

The crystallite size and strain for La-doped $NaVOPO_4$ (NVP-La) are calculated using the maximum intense peak observed at $2\theta = 27.4^{\circ}$. The crystallite size calculated from the XRD pattern of NVP-La is 56.73 which is slightly lower than the NVP-pure which is shown in the Table 4.4.

4.2.1.5. XRD Analysis for Ti-doped $NaVOPO_4$ (NVP-Ti)

XRD pattern of NVP-Ti are in good agreement with the pure phase of $NaVOPO_4$ with a monoclinic crystal structure.

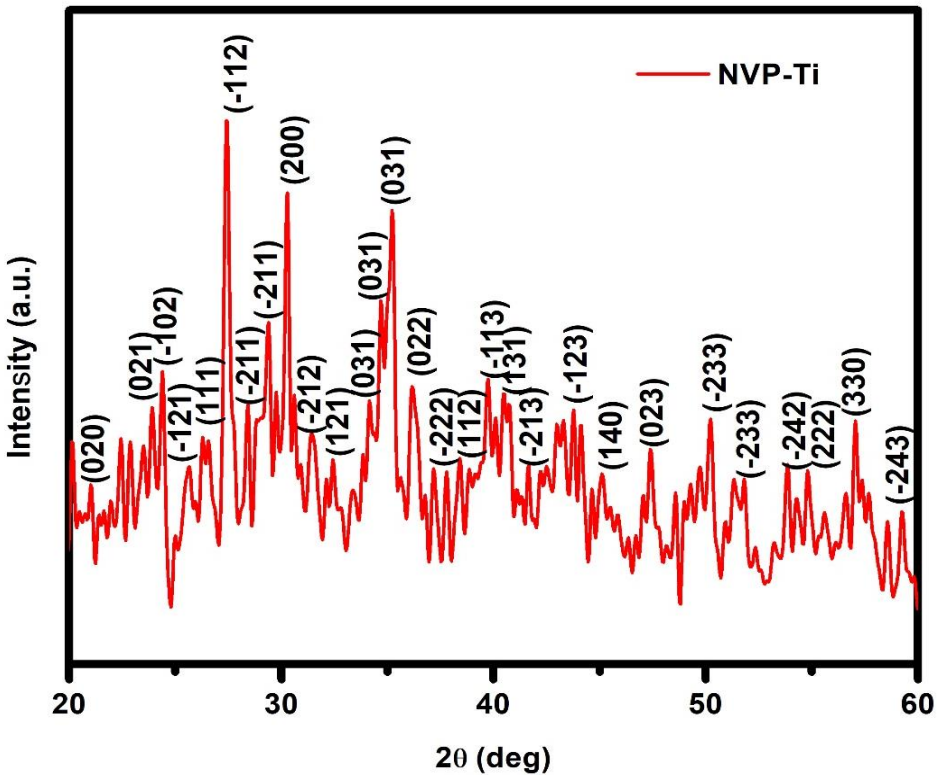

Figure 4.5. XRD pattern of NVP-Ti

The first major diffraction peak observed for Ti-doped $NaVOPO_4$ (NVP-Ti) from the XRD pattern is 27.3˚ and it exactly matches with the major peak of pure $NaVOPO_4$. The corresponding miller indices for the first major peak of Ti-doped $NaVOPO_4$ (NVP-La) is (-112). The other peaks are also matched with the JCPDS card no.76-0417 but the intensity of the diffraction peak alone changes. The XRD pattern of Ti-doped $NaVOPO_4$ (NVP-Ti) is shown in Figure 4.5.

Table 4.5. Parameters obtained from the major peak of the XRD pattern of NVP-Ti

Sample name	2θ (deg)	FWHM β (deg)	Crystallite size (nm)	Strain
NVP-Ti	**27.3**	**1.435**	**5.9981**	**2.9052**

The crystallite size and strain for Ti-doped $NaVOPO_4$ (NVP-Ti) are calculated using the maximum intense peak observed at $2\theta = 27.3˚$. The crystallite size observed from the XRD pattern of NVP-Ti is 5.9981 which is very much lesser than the pure phase of $NaVOPO_4$ (NVP-pure).

From the XRD analysis of all the samples, the major peak at 27.3˚ with hkl planes are indexed in Cu doped-NVP, Zr doped-NVP, La doped-NVP and Ti doped-NVP, hence proving that upon addition of dopants in NVP lattice, the structure is preserved so that the performance can be observed. In the case of Zr-doped NVP, an oriented structure along (200) plane is observed.

The crystallite size of NVP-pure is 61.18 nm and it has decreased in the order of NVP-La > NVP-Zr > NVP-Cu > NVP-Ti where the crystallite size of titanium doped with NVP is 5.9981 nm which is comparatively low when compared to NVP-pure. A similar match of peaks are observed for all the NVP samples as that of pure NVP which indicates that upon doping of di and tri valent elements, a structural stability is maintained except for Zr-doped sample getting specific orientation along (022).

4.3 Cyclic Voltammetric (CV) Analysis

Cyclic Voltammtery (CV) analysis for NVP-pure, NVP-Cu, NVP-Zr, NVP-La and NVP-Ti are performed using Biologic SP-150 electrochemical workstation. Cyclic voltammetry is used to determine the reversibility of a reaction, the diffusion coefficient, oxidation potential and reduction potential of the sample.

4.3.1. Cyclic Voltammetry analysis of NVP-pure

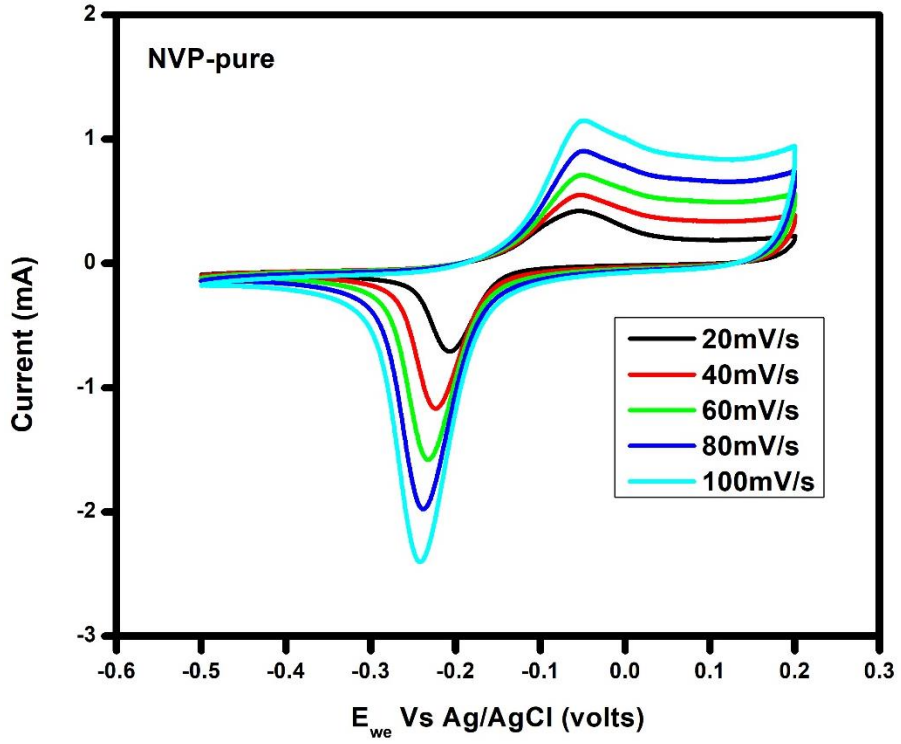

Figure 4.6. CV profile of pure NVP with 1M NaOH electrolyte

Figure 4.6. shows the CV profile of pure NVP with the electrolytic concentration of 1M-NaOH at different scan rates ranging from 20mV/s to 100mV/s. With NaOH electrolyte, NVP exhibits a broad redox peak, because Na^+ has the highest ionic conductivity than Lithium and OH^- has the highest ionic conductivity than anions. The redox activity is observed in the potential window, -0.5 V to 0.2 V. The oxidation and the reduction peaks for NVP-pure are observed at -0.0489 V and -0.2398 V.

The diffusion coefficient is calculated by using the formula,

$$\mathbf{D} = \left(\frac{\boldsymbol{B}}{\mathbf{2.69\times10^5}\ \boldsymbol{A\ Cn^{3/2}}}\right)^2$$

where,

B – slope of the linear plot (mole/second)

A – Area of the electrode (cm^2)

C – Concentration of the electrolyte (mole/litre)

The diffusion coefficient of the electrochemical cells using the as-prepared sample with NaOH electrolyte is listed in the Table 4.6.

The pre-requisities for a reversible electrochemical system (Nernstian system) are

(i) Unity in peak current ratio

(ii) Linearity between square root of scan rate and peak current,

(iii) Constant peak potential for different scan rate.

(iv) Peak separation more than or equal to 59 mV.

Table 4.6. CV analysis of NVP-pure at an electrolytic concentration of 1M-NaOH

Scan rate (mV/s)	**Potential (V)**		**Current (mA)**		**$\lvert E_{red}-E_{ox}\rvert$**	**$\lvert I_{red}/I_{ox}\rvert$**	**Diffusion Coefficient cm^2/s**
	E_{ox}	**E_{red}**	**I_{ox}**	**I_{red}**			
20	-0.0551	-0.2058	0.4019	-0.1464	0.1507	2.1029	Anodic 0.031×10^{-13} S/cm
40	-0.0537	-0.2208	0.5514	-0.1934	0.1671	2.8326	
60	-0.0521	-0.2322	0.7197	-0.2936	0.1801	3.225	
80	-0.0521	-0.2368	-0.8962	-0.4115	0.1847	3.615	Cathodic 3.18×10^{-13} S/cm
100	-0.0489	-0.2398	1.151	-0.4575	0.1909	3.068	

In this electrochemical system of NVP-pure, the peak current ratio of both the systems are slightly greater than one which also indicates the reversible nature of the system.

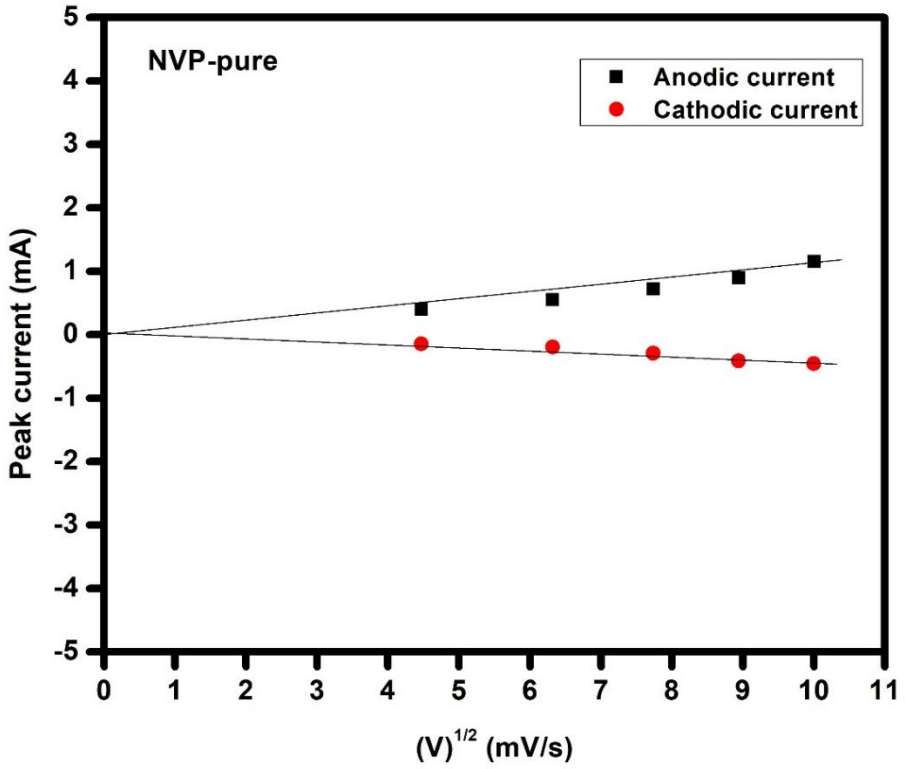

Figure 4.7. Plot of scan rate Vs peak current for NVP-pure

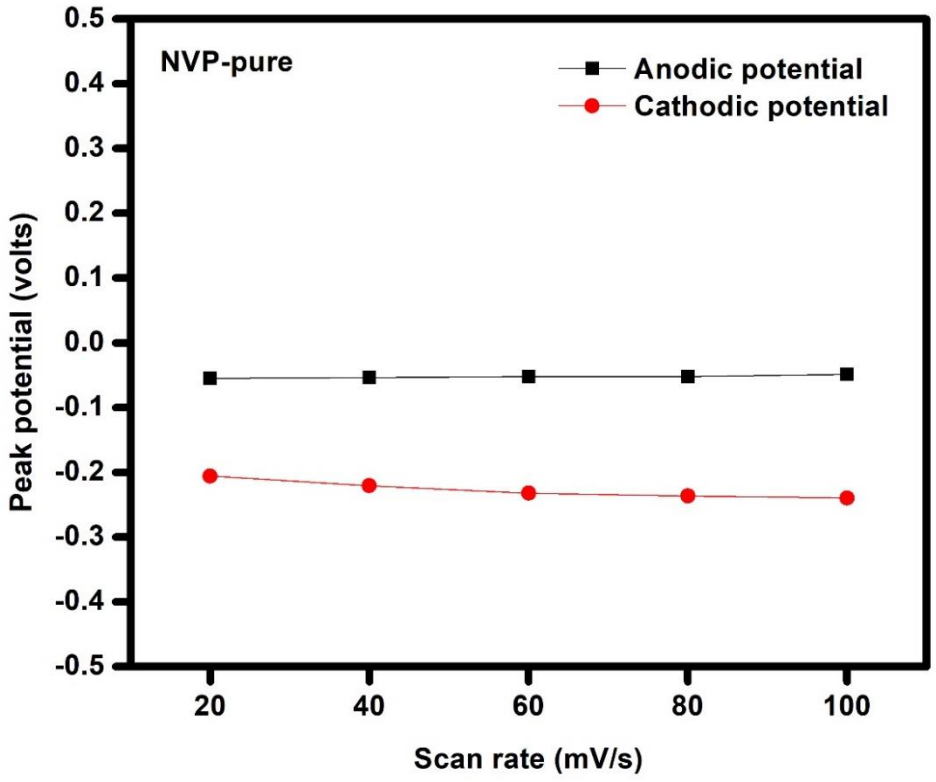

Figure 4.8. Plot of scan rate Vs peak potential for NVP-pure

The linear dependence of square root of scan rate with peak current is evident and the linear points are coinciding well with all the data points and is shown in Figure 4.7.

Independency of peak potential with scan rate is observed from the CV graphs of the as-prepared sample in 1M NaOH electrolytic solution for different scan rates and is shown in Figure 4.8. respectively.

4.3.2. Cyclic Voltammetry analysis for Cu-doped NVP (NVP-Cu)

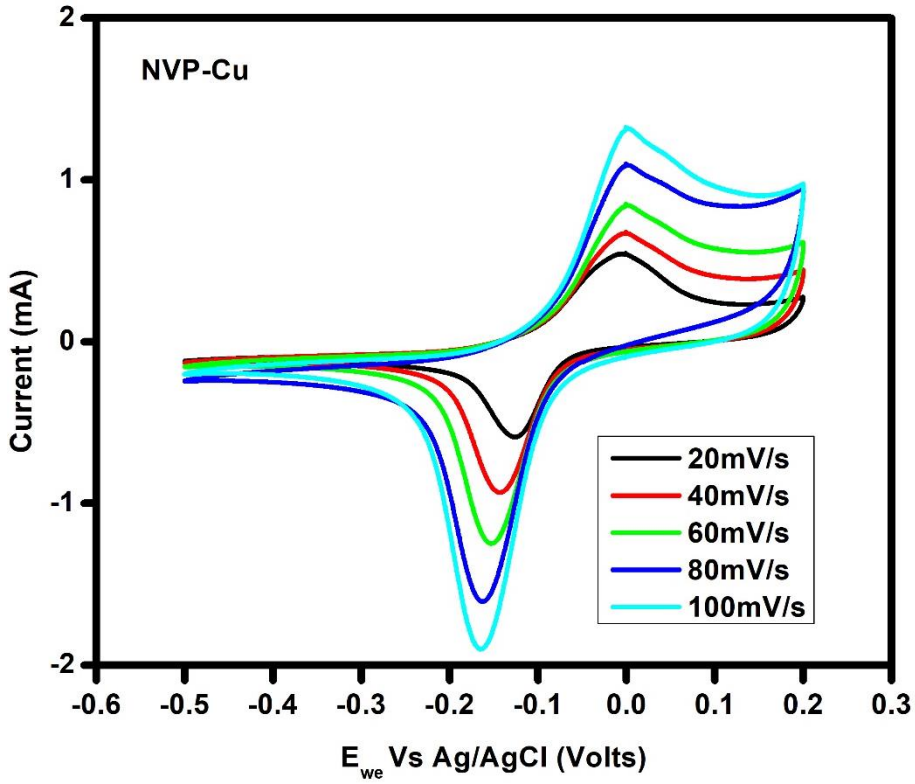

Figure 4.9. CV profile of NVP-Cu with 1M NaOH electrolyte

Figure 4.9. shows the CV profile of NVP-Cu with the electrolytic concentration of 1M-NaOH at different scan rates ranging from 20mV/s to 100mV/s.

The oxidation and reduction peaks are observed for 100 mV/s of NVP-Cu are observed at 0.0006 and -0.168 V, respectively. The potential window of the prepared sample in 1M NaOH electrolyte lies between -0.5 to +0.2 V.

The diffusion coefficient of the electrochemical cells using the as-prepared sample with NaOH electrolyte is listed in the Table 4.7.

Table 4.7. CV analysis of NVP-Cu at an electrolytic concentration of 1M-NaOH

Scan rate (mV/s)	Potential (V)		Current (mA)		$\lvert E_{red}-E_{ox}\rvert$	$\lvert I_{red}/I_{ox}\rvert$	Diffusion Coefficient cm^2/s
	E_{ox}	E_{red}	I_{ox}	I_{red}			
20	-0.0045	-0.1245	0.3862	-0.4647	0.12	1.2032	Anodic 0.067×10^{-13} S/cm
40	-0.0045	-0.1441	0.4113	-0.7255	0.1396	1.7639	
60	-0.0011	-0.153	0.4815	-1.0095	0.1513	2.09657	
80	-0.0019	-0.1636	0.5363	-1.8842	0.1617	3.5133	Cathodic 0.047×10^{-15} S/cm
100	-0.006	-0.168	0.6817	-1.5832	0.1620	2.322	

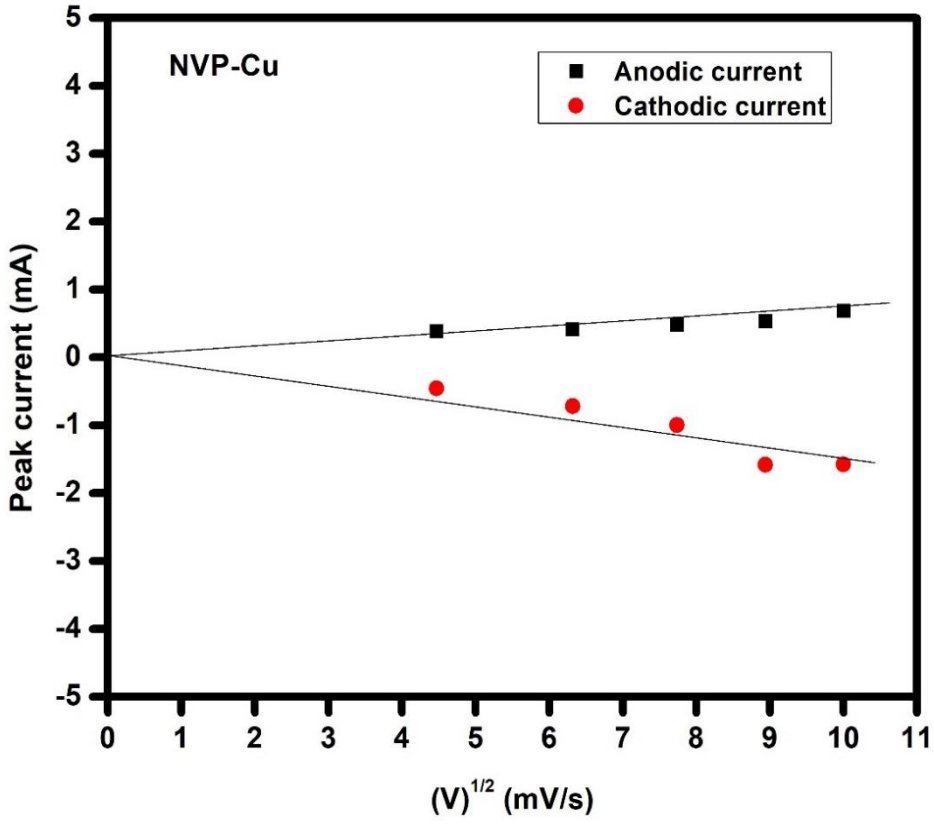

Figure 4.10. Plot of scan rate Vs peak current for NVP-Cu

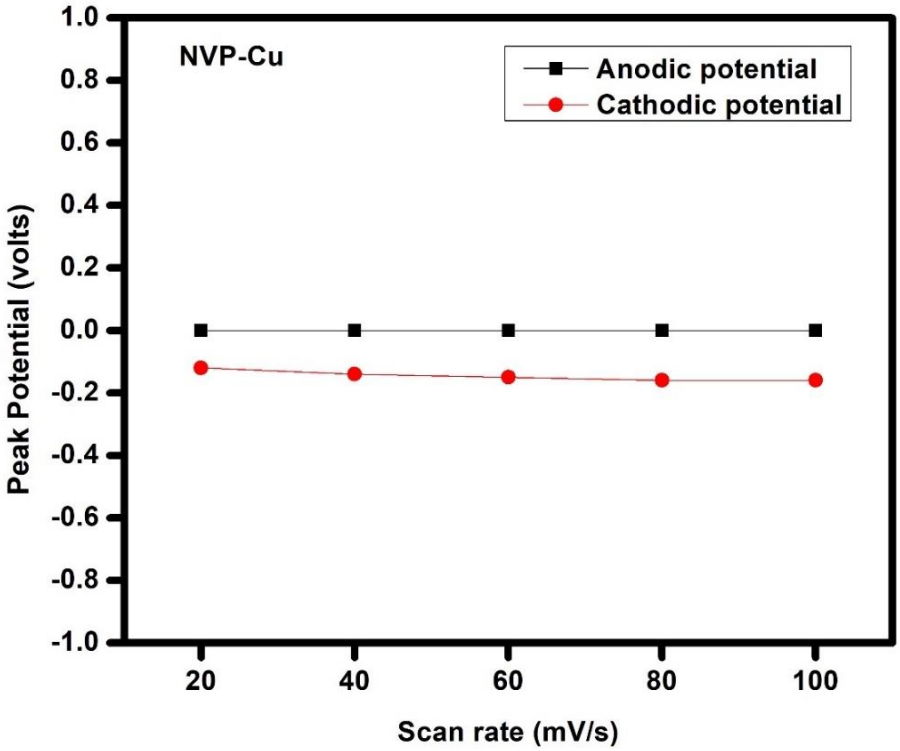

Figure 4.11. Plot of scan rate Vs peak potential for NVP-Cu

The linear dependence of square root of scan rate with peak current is evident and the linear points are coinciding well with all the data points and is shown in Figure 4.10.

Independency of peak potential with scan rate is observed from the CV graphs of the as-prepared NVP-Cu sample in 1M NaOH electrolytic solution for different scan rates and is shown in Figure 4.11. respectively.

4.3.3. Cyclic Voltammetry analysis for Zr doped NVP (NVP-Zr)

Figure 4.12. shows the CV profile of NVP-Zr with the electrolytic concentration of 1M-NaOH at different scan rates ranging from 10mV/s to 100mV/s.

The oxidation and reduction peaks for 100 mV/s of NVP-Zr are observed at -0.0683 and -0.25 V. The potential window of the prepared sample in NaOH electrolyte lies between -0.5 to +0.2 V. The diffusion coefficient of the electrochemical cells using the as-prepared NVP-Zr sample with NaOH electrolyte is listed in the Table 4.8.

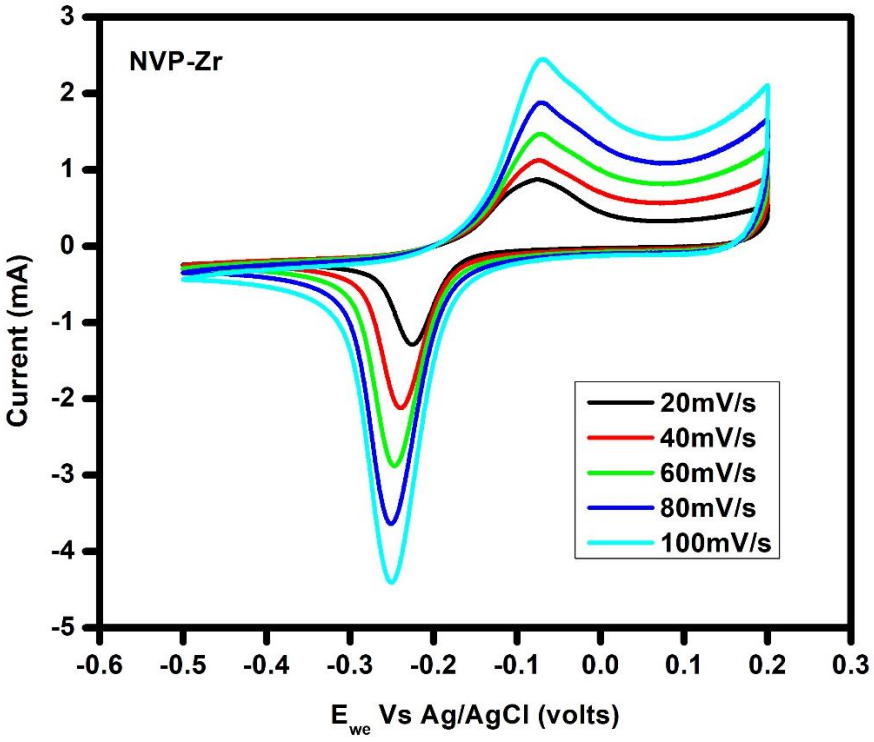

Figure 4.12. CV profile of NVP-Zr with 1M NaOH electrolyte

Table 4.8. CV analysis of NVP-Zr at an electrolytic concentration of 1M-NaOH

Scan rate (mV/s)	Potential (V)		Current (mA)		$\lvert E_{red}-E_{ox}\rvert$	$\lvert I_{red}/I_{ox}\rvert$	Diffusion Coefficient cm^2/s
	E_{ox}	E_{red}	I_{ox}	I_{red}			
20	-0.0735	-0.2274	0.5761	-1.0351	0.1539	1.7967	Anodic 0.03×10^{-13} S/cm
40	-0.0749	-0.2388	0.696	-1.7187	0.1639	2.4693	
60	-0.0733	-0.2452	0.9374	-2.4413	0.1719	5.6043	
80	-0.0733	-0.2452	1.2429	-3.1568	0.1719	2.599	Cathodic 0.21×10^{-13} S/cm
100	-0.0683	-0.25	1.449	-3.7214	0.1817	5.568	

In the case of NVP-Zr, the peak current ratio is higher and is nonlinear at a low scan rate indicating the reversibility can be achieved only in the faster kinetics. The diffusion co-efficient of the Zr-doped NVP is comparatively low than the pure NVP by one order on cathodic side, hence improving the electrochemical performance.

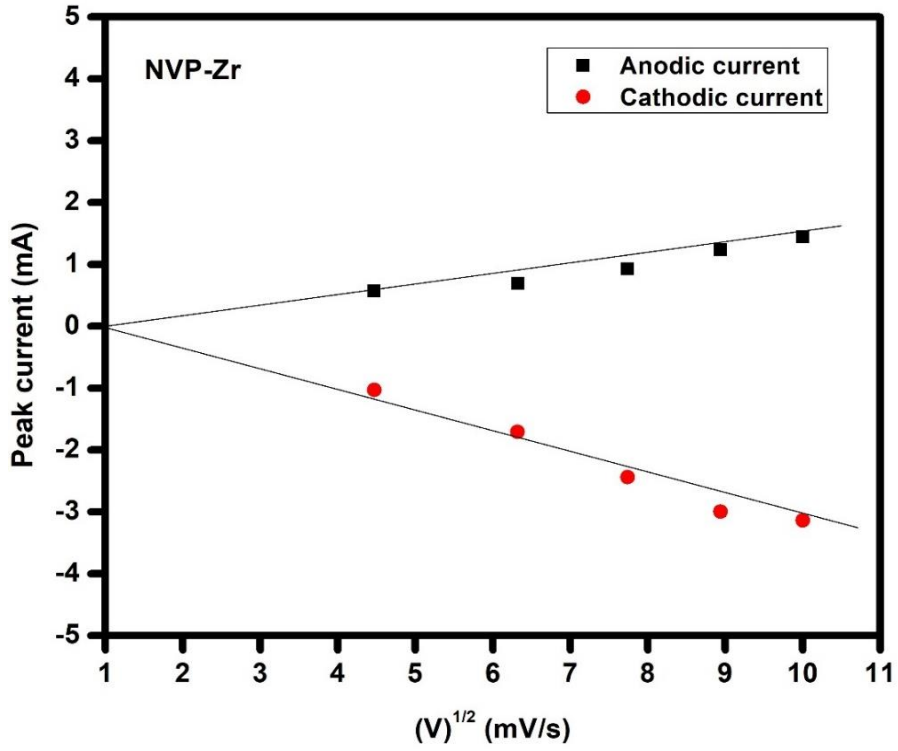

Figure 4.13. Plot of scan rate Vs Peak current for NVP-Zr

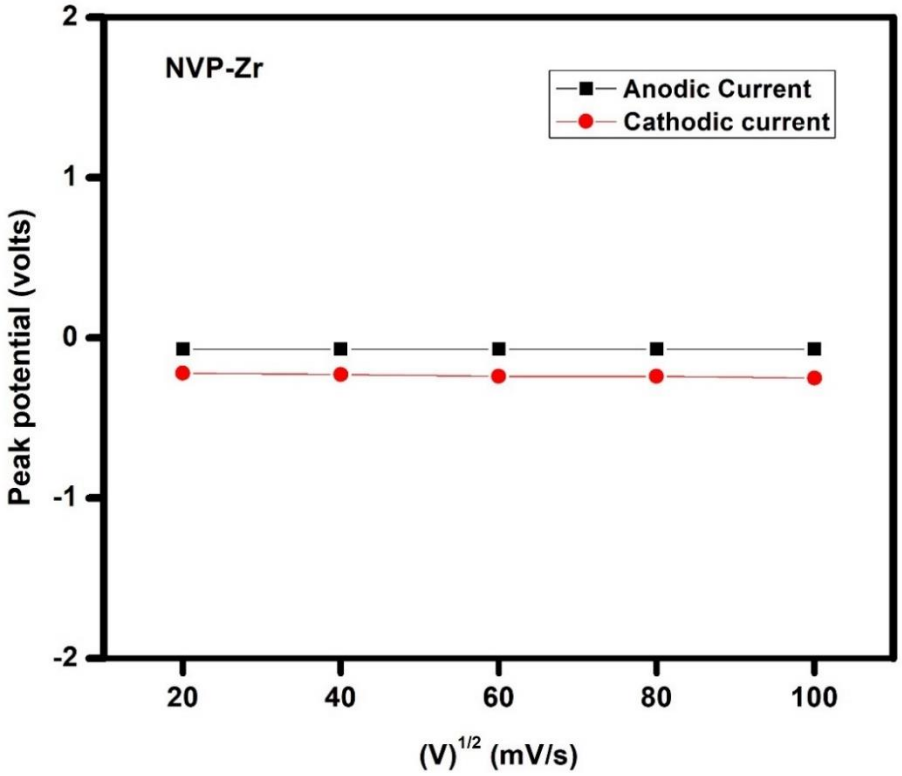

Figure 4.14. Plot of scan rate Vs peak potential for NVP-Zr

Independency of peak potential with scan rate is observed from the CV graphs of the as-prepared NVP-Zr sample in 1M NaOH electrolytic solution for different scan rates is shown in Figure 4.14. respectively.

4.3.4. Cyclic Voltammetry analysis for La doped NVP (NVP-La)

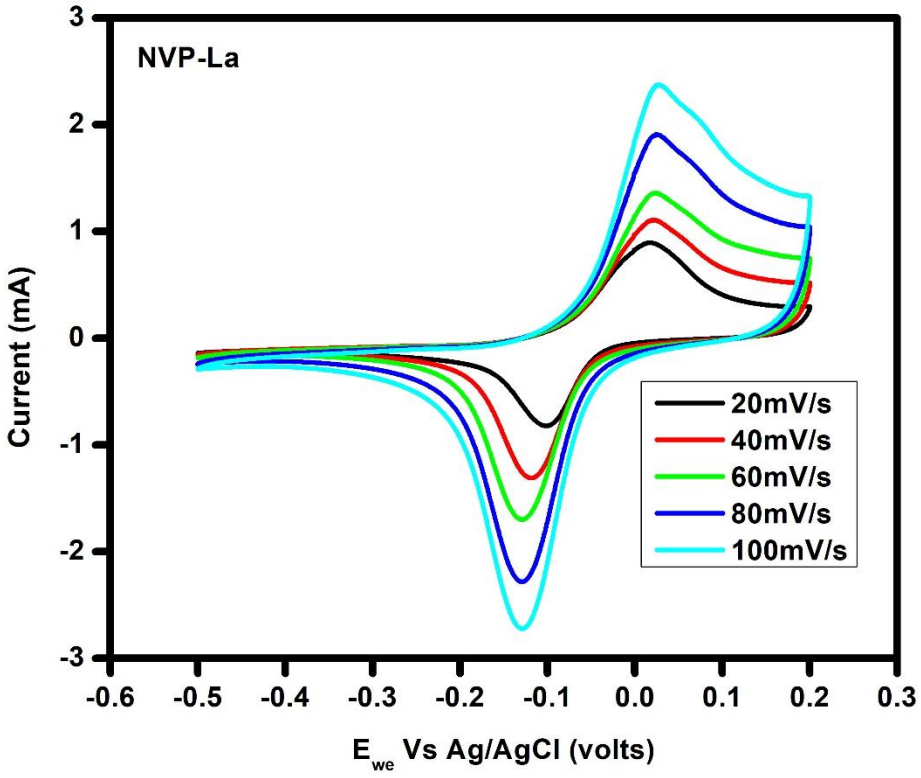

Figure 4.15. CV profile of NVP-La in 1M NaOH with electrolyte

Figure 4.10. shows the CV profile of NVP-La with the electrolytic concentration of 1M-NaOH at different scan rates ranging from 10mV/s to 100mV/s.

The potential window of the prepared sample in NaOH electrolyte lies between -0.5 to +0.2 V.

The diffusion coefficient of the electrochemical cells using the as-prepared NVP-La sample with NaOH electrolyte is listed in the Table 4.9.

Table 4.9. CV analysis of NVP-La at an electrolytic concentration of 1M-NaOH

Scan rate (mV/s)	Potential (V)		Current (mA)		$\lvert E_{red}-E_{ox}\rvert$	$\lvert I_{red}/I_{ox}\rvert$	Diffusion Coefficient cm^2/s
	E_{ox}	E_{red}	I_{ox}	I_{red}			
20	0.0150	-0.1019	0.624	-0.6774	0.1169	1.0855	
40	0.0206	-0.1165	0.6152	-1.3085	0.1371	2.1269	Anodic
60	0.0258	-0.1263	0.7805	-1.3992	0.1521	1.7926	0.023×10^{-13} S/cm
80	0.2286	-0.1353	1.0726	-1.8523	0.6339	1.7269	Cathodic
100	0.0292	-0.1281	1.2623	-2.214	0.1573	1.7539	0.044×10^{-13} S/cm

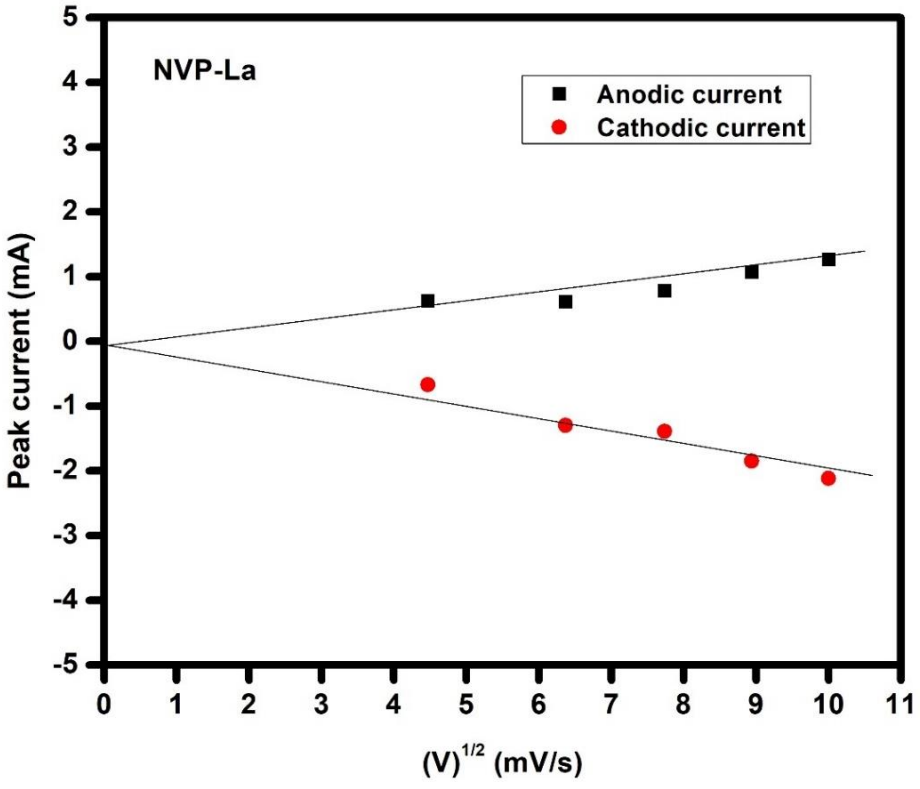

Figure 4.16. Plot of scan rate Vs peak current for NVP-La

Independency of peak potential with scan rate is observed from the CV graphs of the as-prepared sample in 1M NaOH electrolytic solution for different scan rates is shown in Figure 4.12**.,** respectively

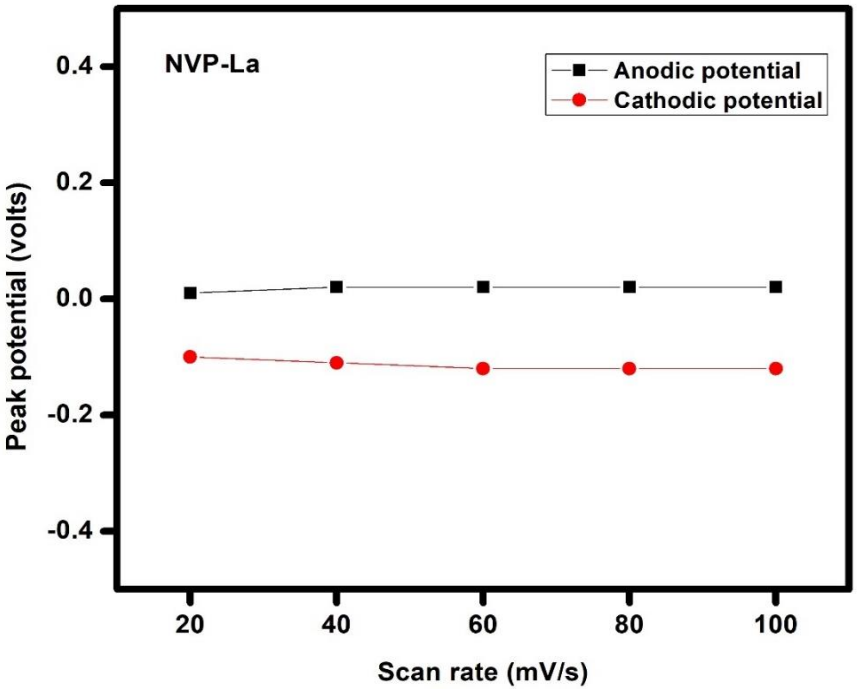

Figure 4.17. Plot scan rate and peak potential for NVP-La

4.3.5. Cyclic Voltammetry analysis for Ti doped NVP (NVP-Ti)

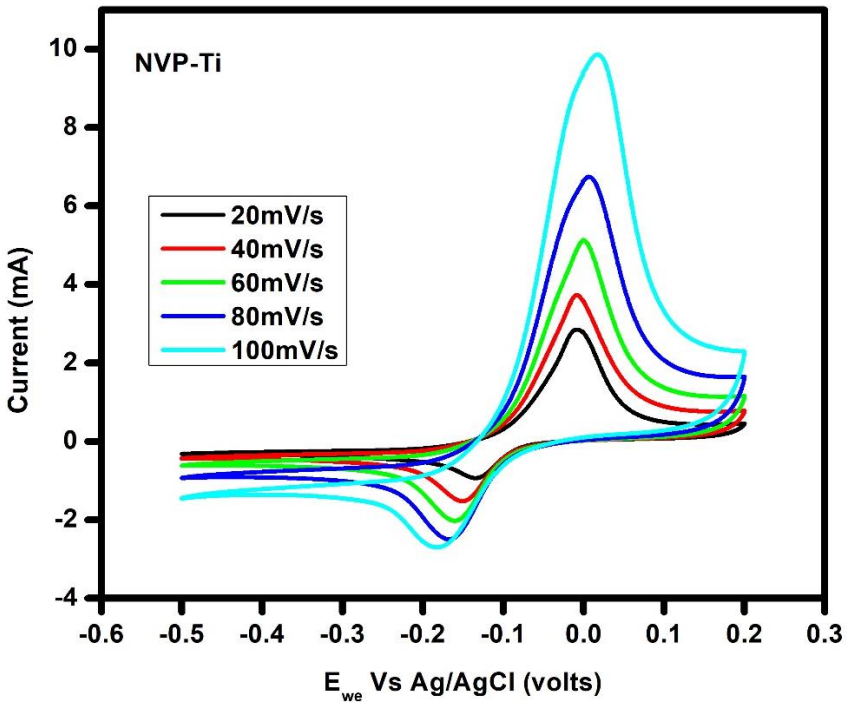

Figure 4.18. CV profile of NVP-Ti in 1M NaOH with electrolyte

Figure 4.18. shows the CV profile of NVP-Ti with the electrolytic concentration of 1M-NaOH at different scan rates ranging from 10mV/s to 100mV/s.

The oxidation and the reduction peaks for 100 mV/s of NVP-Ti are observed at 0.017 and -0.1176 V respectively. The potential window of the prepared sample in NaOH electrolyte lies between -0.5 to +0.2 V. The diffusion coefficient of the electrochemical cells using the as-prepared sample with NaOH electrolyte is listed in the Table 4.1.

Table 4.10. CV analysis of NVP-Ti at an electrolytic concentration of 1M-NaOH

Scan rate (mV/s)	Potential (V)		Current (mA)		$\lvert E_{red}-E_{ox}\rvert$	$\lvert I_{red}/I_{ox}\rvert$	Diffusion Coefficient cm^2/s
	E_{ox}	E_{red}	I_{ox}	I_{red}			
20	-0.0109	-0.1333	2.2437	-0.6552	0.1224	0.2920	Anodic 0.716×10^{-13} S/cm
40	-0.0099	-0.1510	2.9774	-1.1541	0.1410	0.3876	
60	-0.0025	-0.1576	4.1226	-1.3103	0.1551	0.31	
80	0.0096	-0.1640	5.3264	-1.7044	-0.1544	0.3199	Cathodic 0.0498×10^{-13} S/cm
100	0.017	-0.1776	7.6678	-1.5446	-0.1606	0.2014	

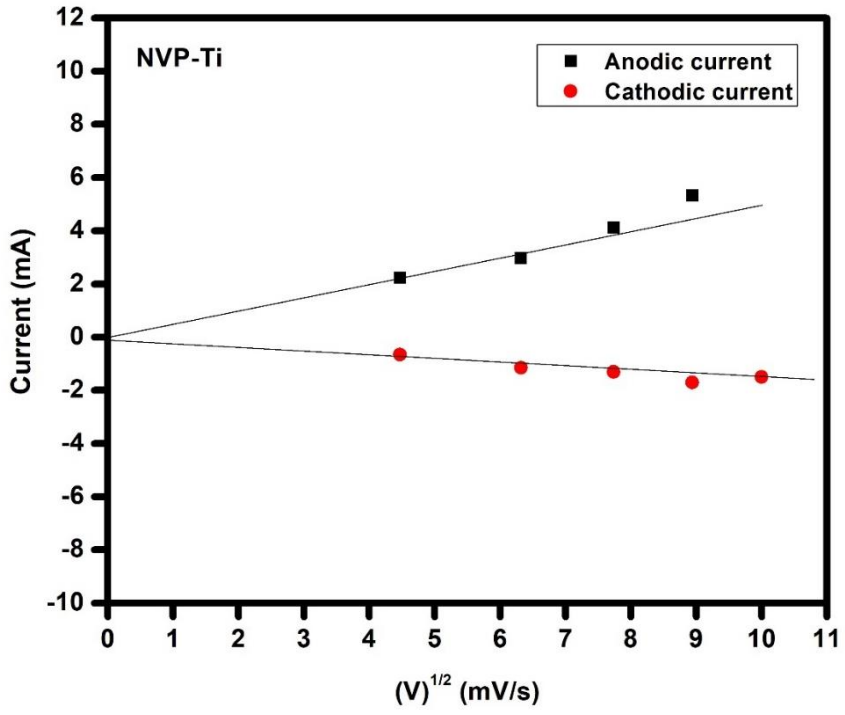

Figure 4.19. Plot of scan rate Vs peak current for NVP-Ti

In this electrochemical system, the peak current ratio of the anode is greater than two and it shows the irreversibility of the NVP-Ti sample, Figure 4.19.

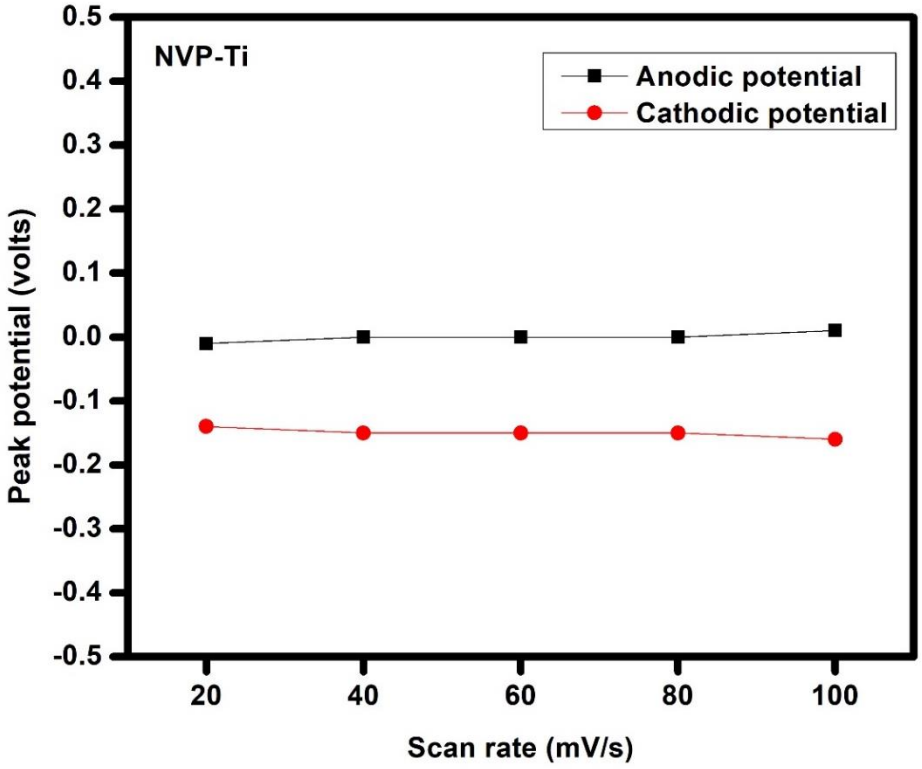

Figure 4.20. Plot scan rate and peak potential for NVP-Ti

Independency of peak potential with scan rate is observed from the CV graphs of the as-prepared NVP-Ti sample in 1M NaOH electrolytic solution for different scan rates is shown in Figure 4.20. respectively.

Hence, among all the samples of NVP, Ti-doped NVP (NVP-Ti) exhibits a higher anodic current of 7.66 mA and highest diffusion anodic current of 0.716 a 10^{-13} than NVP pure and it is also evident to possess a lower crystallite size of 5.99 nm from the XRD analysis.

In the case of pure NVP, a maximum peak current of 0.69 mA is observed and similarly for Cu-doped NVP (NVP-Cu), it is observed at 0.68 mA which do not increase the electrochemical activity and the diffusion co-efficient does not show any increase than the pure NVP. But for Zr-doped NVP, the diffusion co-efficient on the cathodic side shows a higher value than pure NVP and a maximum current of 1.44 mA is observed. For La-doped (NVP-La), the maximum current is obtained at 1.26 mA nearly like Zr-doped NVP (NVP-pure) NVP-Zr and the diffusion co-efficient does not show any increase from NVP-pure.

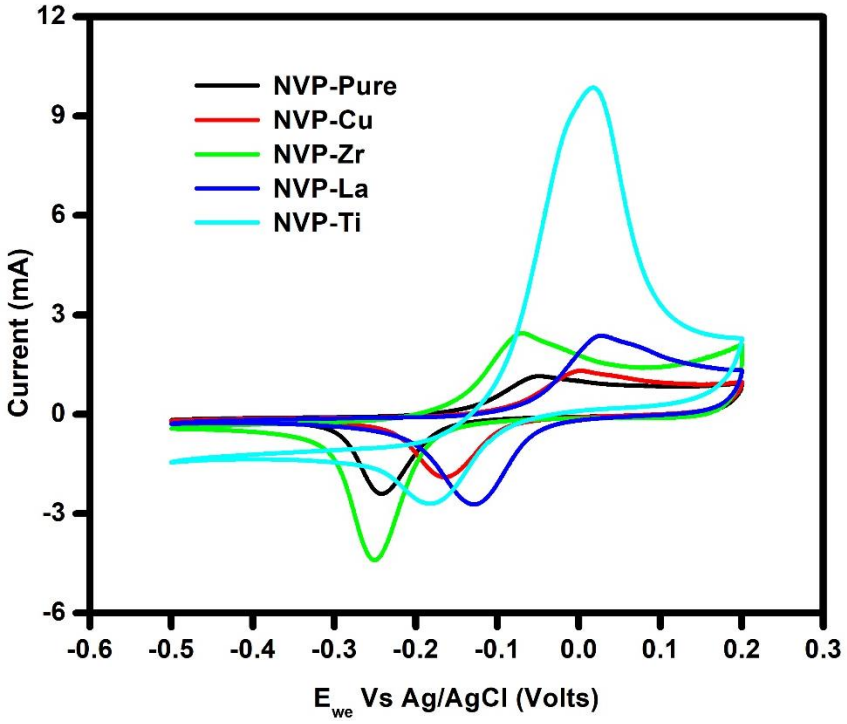

Figure 4.21. Comparison graph of NVP-pure, NVP-Cu, NVP-Zr, NVP-La and NVP-Ti at 100 mV/s

With regard to the Ti-doped NVP (NVP-Ti), a higher maximum current of 7.66 mA is observed at the scan rate of 100 mV/s and it shows well resolved redox peaks than the other samples. The linearity between square root of scan rate vs peak current shows a deviated behaviour and the peak current ratio is less than one. Hence, it shows a quasi-reversible nature of the system. As an added point, Ti-doped NVP (NVP-Ti) also exhibits a high anodic diffusion co-efficient of 0.7×10^{-13} which shows that good ion movement could be observed upon cycling with Na-based electrolyte.

This work is has accomplished to prepare a monophase $NaVOPO_4$ compound since much reports are not available in the composition of $NaVOPO_4$ without any mixed phase. Hence, it is an achievement to prepare monophase monoclinic structure.

The monophase monoclinic $NaVOPO_4$ (NVP) is successfully prepared and di valent (Cu^{2+}, Zr^{2+}) and tri valent (La^{3+}, Ti^{3+}) dopants are incorporated in the lattice without disturbing the monoclinic structure. The electrochemical evaluation of these samples indicated that Zr dopant is a favourable cathodic material and Ti doped NVP is more favourable as an anode material. The diffusion coefficient is high 0.716×10^{-13}, with Ti dopant.

SUMMARY AND CONCLUSION

CHAPTER V

SUMMARY AND CONCLUSION

Sodium Vanadium phosphate is prepared using sol-gel method. The prepared sample is analyzed for the determination of crystal structure using X-ray diffraction (XRD). XRD analysis confirms the structure of Sodium Vanadium phosphate with reference to JCPDS Card No. 76-0417. Similarly, Copper, Zirconium, Lanthanum and Titanium are doped with NVP and it also matches with the monoclinic structure of $NaVOPO_4$. From the XRD analysis, the crystallite size is decreased in the order of NVP-La > NVP-Zr > NVP-Cu > NVP-Ti where the crystallite size of NVP-Ti is 5.99 nm is comparatively low when compared to NVP-pure. The prepared samples of NVP-pure, NVP-Cu, NVP-Zr, NVP-La and NVP-Ti were tested with 1M-NaOH as electrolyte, Platinum as counter electrode and Ag/AgCl as a reference electrode. The cyclability is tested for 100 cycles for all the samples. From the analysis of cyclic voltammetry, NVP-Ti possess a high anodic current at a scan rate of 100mV/s and it shows a higher current of 7.66 mA at 100 mV/s. Therefore, single monophase $NaVOPO_4$ is prepared successfully and di (Cu^{2+}, Zr^{2+}) and trivalent (La^{3+}, Ti^{3+}) dopants are incorporated in the lattice without disturbing the monoclinic structure. Hence from the obtained results, Ti doped NVP (NVP-Ti) is a good cathode material for Sodium-ion batteries.

REFERENCES

REFERENCES

[1] https://www.britannica.com/technology/battery-electronics.

[2] https://circuitdigest.com/article/different-types-of-batteries

[3] edu/education/science-of-solar/battery-technology

[4] https://www.imeche.org/news/news-article/the-big-battery-challenge-3-potential-alternatives-to-lithium-ion

[5] https://www.thomasnet.com/insights/7-lithium-battery-alternatives/

[6] https://www.euronews.com/green/2022/02/09/we-re-facing-a-lithium-battery-crisis-what-are-the-alternatives

[7] https://www.blackridgeresearch.com/blog/the-future-roadmap-for-sodium-na-ion-batteries

[8] **Wanyu Lu, Zijie Wang, Shuhang Zhong**, Sodium-ion battery technology: Advanced anodes, cathodes and electrolytes, Journal of Physics: Conference Series, 2021, 2109, 012004.

[9] **Xianguang Zeng, Jing Peng, Yi Guo, Huafeng Zhu, Xi Huang**, Research Progress on $Na_3V_2(PO_4)_3$ Cathode Material of Sodium Ion Battery, Frontiers in chemistry, 2020, 8, 635.

[10] https://www.power-and-beyond.com/what-is-a-sodium-ion-battery-definition-structure-

[11] **El Abadila Iffer, Mohammed Belaiche, Chouaib Ahmani Ferdi, Moustapha Elansary, Abdul Khader Sunar, Yanxia Wang, Yuliang Cao**, International Journal of Energy Research, 2020, 45(2), 1703-1719. doi: 10.1002/er.5835.

[12] **Prashanta K. Mukharjee, K. M. Ranjith, B. Koo, J. Sichelschmidt, M. Baenitz, Y. Skourshi, Y. Inagaki, Y. Furukawa, A. A. Tsirlin, R. Nath**, Bose-Einstein Condensation of triplons close to the quantum critical point in the quasi-one-dimensional spin- $\frac{1}{2}$ antiferromagnet $NaVOPO_4$, Physical review B (Covering condensed matter and material physics), 2019, 100(14), 144433, doi: 10.1103/PhysRevB.100.144433.

[13] **Pablo A. Aparicio, James A. Dawson, M. Saiful Islam, and Nora H. de Leeuw**, A Computational Study of $NaVOPO_4$ Polymorphs as Cathode Materials for Na-Ion Batteries: Diffusion, Electronic Properties and Cation Doping Behavior, The Journal of Physical Chemistry, 2018, 122(45), 25829-25836, doi: 10.1021/acs.jpcc.8b07797.

[14] Guang He, Ashfia Huq, Wang Hay Kan, Arumugam Manthiram, β-$NaVOPO_4$ Obtained by a Low-temperature Synthesis Process: A New 3.3 V Cathode for Sodium-ion Batteries, Chemistry of Materials, 2016, 28(5), 1503-1512, doi: 10.1021/acs.chemmater.5b04992.

[15] Chih-Yao Chen, Kazuhiko Matsumoto, Toshiyuki Nohira, Rika Hagiwara, Improved Electrochemical Performance of $NaVOPO_4$ Positive Electrodes at Elevated temperature in an Ionic Liquid Electrolyte, Journal of the Electrochemical Society, 2015, 162(10), A2093-A2098.

[16] Jie spng, Maowen Xu, Long Wang, John B. Goodenough, Exploration of $NaVOPO_4$ Na-ion battery, Chemical Communications, 2013, 29, 5280-5282. doi:10.1039/C3CC42172D**.**

[17] V. Kiran Kumar, Sourav Ghosh, Sanjay Biswas, and Surendra K. Martha, Pitch-Derived Soft-Carbon-Wrapped $NaVPO_4F$ Composite as a Potential Cathode Material for Sodium-Ion Batteries, Applied Energy Materials, 2021, 4(4), 4059-4069, doi: 10.1021/acsaem.1c00410.

[18] Chen-DE hao, Jin-Zhi Guo, Xin-Xin Zhao, Wen-Hao Li, Xu Yang, Hao-Jie Liang, Xing-Long Wu, Robust three-dimensional carbon conductive network in $NaVPO_4F$ cathode towards superior high-rate and ultralong-lifespan sodium-ion full batteries, Journal of Materials Chemistry, 2020, 8, 17454-17462, doi: 10.1039/D0TA06614A.

[19] Xiaochen Ge, Xinhai Li, Zhixing Wang, Huajun Guo, Guochun Yan, Xianwen Wu, Jiexi Wang, Facile synthesis of $NaVPO_4F$/C cathode with enhanced interfacial conductivity towards long-cycle and high-rate sodium-ion batteries, Chemical Engineering Journal, 2018, 357, 458-462, doi: 10.1016/j.cej.2018.09.099.

[20] Markas Law, Palani Balaya, $NaVPO_4F$ with High Cycling Stability as a Promising Cathode for Sodium-ion Battery, Energy Storage Materials, 2018, 10, 102-113, doi: 10.1016/j.ensm.2017.08.007.

[21] Pingyuan Feng, Wei Wang, Jie Hou, Kangli Wang, Shujie Chang, Kai Jiang, A 3D coral -like structured $NaVPO_4F$/C constructed by a novel synthesis route as high-performance cathode material for sodium-ion battery, Chemical Engineering Journal, 2018, 353, 25-33, doi: 10.1016/j.cej.2018.07.114

[22] J. Barker, M. Y. Saidi, J. L. Swoyer, A Sodium-Ion Cell Based on the Fluorophosphate Compound $NaVPO_4F$, Electrochemical and SolidState Letters, 2003, 6(1), A1-A4. doi:10.1149/1.1523691.

[23] Yongjin Fang, Jiexin Xhang, Faping Zhong, Xiangming Feng, WEihua Chen, Xinping Ai, Hanxi Yang, Yuliang Cao, Amorphous $NaVOPO_4$ as a High-Rate and Ultrastable Cathode Material for Sodium-ion Batteries, Chinese Chemical Society, 2021, 3(10), 2428-2436, doi: 10.31635/ccschem.020.202000520**.**

[24] Yongjin Fang, Qi Liu, Lifen Xiao, Xianran Xing, Xianghui Xiao, Yang Ren, A Fully Sodiated $NaVOPO_4$ with Layered Structure for High-Voltage and Long-Lifespan Sodium-Ion Batteries, A Cell Press Journal, 2018, 4(5), 1167-1180, doi: 10.1016/j.chempr.2018.03.006.

[25] Yang Ni, Guang He, Stable cycling of β-$VOPO_4$/$NaVOPO_4$ cathodes for sodium-ion batteries, Electrochimica Acta, 2018, 292, 47-54, doi: 10.1016/j.electacta.2018.09.140.

[26] HOU Baoxiu, MA Linlin, ZANG Xiaohuan, SHANG Ningzhao, SONG Jianmin, ZHAO Xiaoxian, WANG Chun, QI Jian, WANG Jiangyan YU Ranbo HOU Baoxiu, MA Linlin, ZANG Xiaohuan, SHANG Ningzhao, SONG Jianmin, ZHAO Xiaoxian, WANG Chun, QI Jian, WANG Jiangyan3 and YU Ranbo, Chemical Research in Chinese Universities, 2021, 37, 265-273, doi: 10.1007/s40242-021-0433-y.

[27] Xiaohong Liu, Guilin Feng, Zhenguo Wu, Zuguang Yang, Shan Yang, Xiaodong Guo, Shuaihua Zhang, Xingtao Xu, benhe Zhong, Yusuke Yamauchi, Enhanced Sodium Storage Property of Sodium Vanadium Phosphate via Simultaneous Carbon Coating, 2020, 386, 123953, doi: 10.1016/j.cej.2019.123953.

[28] Nali Li, Yanwei Tong, Dawei Yi, Xumei Cui, Xuefeng Zhang, 3D interconnected porous carbon coated $Na_3V_2(PO_4)_3$/C composite cathode materials for sodium-ion batteries, Ceramic International, 2020, 46(17), 27493-27498, doi: 10.1016/j.ceramint.2020.07.238.

[29] Qizhen Zhu, Xiaqing Chang, Ning Sun, Renjie Chen, Yineng Zhao, Bin Xu, Feng Wu, Confined growth of nano-$Na_3V_2(PO_4)_3$ in porous carbon framework for high-rate Na-ion storage, American Chemical Society, 2019, 11(3), 3107-3115, doi: 10.1021/acsami.8b19614.

[30] Xuemei Li, Shijian Wang, Xiao Tang, Rui Zang, Peng Li, Pengxin Li, Zengming Man, Cong Li, Shuaishuai Liu, Yuhan Wu, Guoxiu Wang, Porous $Na_3V_2(PO_4)_3$/C nanoplates for high-performance sodium storage, Journal of Colloid and Interface Science, 2019, 539, 168-174, doi: 10.1016/j.jcis.2018.12.071.

[31] Yanjun Chen, Youlong Xu, Xiaofei Sun, Chao Wang, Effect of Al substitution on the enhanced electrochemical performance and strong structure stability of $Na_3V_2(PO_4)_3$/c composite cathode for sodium-ion batteries, Journal of Power Sources, 2018, 375, 82-92, doi: 10.1016/j.jpowsour.2017.11.043.

[32] Yanli Ruan, Jingjing Liu, Shidong Song, Ningyi Jiang, Vincent Battaglia, Multi-hierarchical nanosheet-assembled chrysanthemum-structured $Na_3V_2(PO_4)_3$/ C as electrode materials for high-performance sodium-ion batteries, Ionics, 2018, 24, 1663-1673, doi: 10.1007/s11581-017-2342-0.

[33] Hezhang Chen, Yingde Huang, Gaoqiang Mao, Hui Tong, Wangjing Yu, Junchao Zheng, Zhiying Ding, Reduced Graphene Oxide Decorated $Na_3V_2(PO_4)_3$ Microspheres as Cathode Material with Advanced Sodium Storage performance, Physical Chemistry and Chemical Physics, 2018, 6, doi: 0.3389/fchem.2018.00174.

[34] Yilin Zhao, Xinxin Cao, Guozhao Fang, Yaping Wang, Hulin Yang, Shuquan Liang, Anqiang Pan, Guozhong Cao, Hierachically Carbon-coated $Na_3V_2(PO_4)_3$ Nanoflakes for High-Rate Capability and Ultralong Cycle-Life Sodium Ion Batteries, Chemical Engineering Journal, 2018, 339, 162-169, doi: 10.1016/j.cej.2018.01.088.

[35] Xiaohong Liu, Enhui Wang, Guilin Feng, Zhenguo Wu, Wei Xiang, Xiaodong Guo, Juntao Li, Benhe Zhong, Zhuo Zheng, Compared investigation of carbon-decorated $Na_3V_2(PO_4)_3$ with saccharides of different molecular weights as cathode of sodium ion batteries, Electrochimica Acta, 2018, 286, 231-241, doi: 10.1016/j.electacta.2018.08.052.

[36] Zifan Zhou, Na Li, Chi Zhang, Xin Chen, Feng Xu, Chao Peng, $Na_3V_2(PO_4)_3$ nanoparticles encapsulated in carbon nanofibers with excellent Na+ storage for sodium-ion batteries, Solid State Ionics, 2018, 326, 77-81, doi: 10.1016/j.ssi.2018.09.016.

[37] Ling Wu, Yueying Hao, Shaonan Shi, Xiaoping Zhang, Huacheng Li, Yulei Sui, Liu Yang, Shengkui Zhong, Controllable synthesis of $Na_3V_2(PO_4)_3$/C nanofibers as cathode material for sodium-ion batteries by electrostatic spinning, Sec. Physical Chemistry and Chemical Physics, 2018, 6, doi: 10.3389/fchem.2018.00617.

[38] Ling Wu, Shaonan Shi, Xiaoping Zhang, Yan Yang, Jiequn Liu, Shibao Tang, Shengkui Zhong, Room-temperature pre-reduction of spinning solution for the synthesis of $Na_3V_2(PO_4)_3$/C nanofibers as high-performance cathode materials for Na-ion batteries, Electrochimica Acta, 2018, 274, 233-241, doi: 10.1016/j.electacta.2018.04.122.

[39] Enhui Wang, Wei Xiang, Ranjusha Rajagopalan, Zhenguo Wu, Junghoon Yang, Minzhe Chen, Benhhe Zhong, Shi Xue Dou, Shulei, Xiaodong Guo, Yong-Mook Kang, Construction of 3D Pomegranate-Like $Na_3V_2(PO_4)_3$/ conducting carbon composites for high power sodium ion batteries, Journal of Materials Chemistry, 2017, 5, 9833-9841, doi: 10.1039/C7TA00153C.

[40] M.J. Aragon, J. Gutierrez, R. klee, P. Lavela, R. Alcantra, J.L Tirado, On the effect of carbon content for achieving a high performing $Na_3V_2(PO_4)_3$/c nanocomposoite as cathode for sodium-ion batteries, Journal of Electroanalytical Chemistry, 784, 2017, 47-54, doi: 10.1016/j.jelechem.2016.11.064.

[41] Shaonan Shi, Ling Wu, Yong Hu, Jiabin Chen, Xiaoping Zhang, Jiequn Liu, Shengkui Zhong, $Na_3V_2(PO_4)_3$/C cathode material synthesized by normal temperature chemical reduction and sodiation method, Materials Letters, 2017, 198, 128-131, doi: 10.1016/j.matlet.2017.04.017.

[42] Shiqi Sun, Yanjun Chen, Jun Cheng, Zeyi Tian, Chao Wang, Guangping Wu, Changcheng Liu, Yanzhong Wang, Li Guo, Constructing dimensional gradient structure of $Na_3V_2(PO_4)_3$/C@CNTs-WC by wolfram substitution for superior sodium storage, Chemical Engineering Journal, 2021, 420, 130453, doi: 10.1016/j.cej.2021.130453**.**

[43] Zeyi Tian, Yanjun Chen, Jun Cheng, Shiqi Sun, Chao Wang, Zhenfeng He, Xiaofeng Shi, Yanzhong Wang, Li Guo, Boosting the rate capability and working lifespan of K/Co co-doped $Na_3V_2(PO_4)_3$/C for sodium ion batteries, Ceramics International, 2021, 47(15), 22025-22034, doi: 10.1016/j.ceramint.2021.04.222.

[44] Guo-dong Yi, Investigation Writing – original draft Visualization, Chang-ling Fan, Methodology Writing – review & editing Supervision, Zhuang Hu, Wei-hua Zhang, Shao-chang Han, Jin-shui Liu, Construction of high-performance N-doped $Na_3V_2(PO_4)_2F_3$/C cathode assisting by plasma enhanced chemical vapor deposition for sodium-ion batteries, Electrochimica Acta, 2021, 383, 138370, doi: 10.1016/j.electacta.2021.138370.

[45] Nitheesha Shaji, Murugan Nanthagopal, Chang Won Ho, Chang Woo Lee, Effect of chitosan-derived nitrogen-doped carbon surface modification on $Na_3V_2(PO_4)_3$ cathode for rechargeable sodium-ion batteries, Journal of Environmental Chemical Engineering, 2021, 9, 106319, doi: 10.1016/j.jece.2021.106319.

[46] Zhaoyang Wang, Jinmei Liu, Zijuan Du, Haizheng Tao, Yuanzheng Yue, Enhancing Na-storage in $Na_3V_2(PO_4)_3$/C cathodes for sodium-ion batteries through

Br and N co-doping, Inorganic Chemistry Frontiers, 2020, 7(5), 1289-1297, doi: 10.1039/C9QI01690B.

[47] Xiaoying Liu, Muyi Li, Xiang Yang, Xiang Zeng, Huixian Wan, Hongmei Jiang, Carbon encapsulation and chlorine doping enable $Na_3V_2(PO_4)_3$ superior sodium ion storage properties as cathode material for sodium ion battery, Power Technology, 2020, 364, 70-77, doi: 10.1016/j.powtec.2020.01.055.

[48] Jin An Sam Oh, Hongying He, Jianguo Sun, Xun Cao, Bengwah Chua, Yizhong Huang, Kaiyang Zeng, and Li Lu, Dual Nitrogen-doped Carbon Decorated on $Na_3V_2(PO_4)_3$ To Stabilize Three Sodium Ions Intercalation, ACS Applied Energy Materials, 2020, 3(7), 6870-6879, doi: 10.1021/acsaem.0c00973.

[49] Jiahao Li, Jun Cheng, Yanjun Chen, Chao Wang, Li Guo, Effect of K/Zr co-doping on the elevated electrochemical performance of $Na_3V_2(PO_4)_3$/C cathode material for sodium ion batteries, Ionics, 2020, 27, 181-190, doi: 10.1007/s11581-020-03791-3.

[50] Bi, Xiaoqing Liu, Xiaoyan Li, Bingbing Chen, Qiaoji Zheng, Fengyu Xie, Yu Huo, and Dunmin Lin, Modulation of the Crystal Structure and Ultralong Life Span of a $Na_3V_2(PO_4)_3$-Based Cathode for a High-Performance Sodium-Ion Battery by Niobium−Vanadium Substitution, Industrial & Engineering Chemistry Research, 2020, 59(48), 21039-21046, doi: 10.1021/acs.iecr.0c04187.

[51] Yu Gu, Furen Xiao, Kai Xu, Xiaoyan Pan, Jin Li, Caiyun Xu, Xiaodong Zhou, Outstanding electrochemical performance of sodium vanadium phosphate cathode co-modified by carbon-coating and titanium-doping for Na-ion batteries, Ceramic International, 2019, 45(9), 12570-12574, doi: 10.1016/j.ceramint.2019.03.074**.**

[52] Wei Li, Zhujun Yao, Cheng-ao Zhou, Xiuli Wang, Xinhui Xia, Changdong Gu, Jiangping Tu, Boosting High-Rate Sodium Storage Performance of N-Doped Carbon-Encapsulated $Na_3V_2(PO_4)_3$ Nanoparticles Anchoring on Carbon Cloth, Nano-Micro Small, 2019, 15(43), 1902432, doi: 10.1002/smll.201902432.

[53] Hong-bo Huang, Shao-hua Luob, Cai-ling Liu, Yue Yang, Yu-chun Zhai, Long-jiao Chang, Ming-qi Li, Double-carbon coated $Na_3V_2(PO_4)_3$ as a superior cathode material for Na-ion batteries, Applied Surface Science, 2019, 487, 1159-1166, doi: 10.1016/j.apsusc.2019.05.224.

[54] Haifeng Jiang, Xiaoyi Cai, Zhan Wang, Lili Zhang, Lijun Zhou, Linfei Lai, Xiang Liu, Selection of graphene dopants for $Na_3V_2(PO_4)_3$ graphene composite as high rate, ultra long-life sodium-ion battery cathodes, Electrochmica Acta, 2019, 306, 558-567, doi: 10.1016/j.electacta.2019.03.132.

[55] Junqi Fang, Suqing Wang, Xiang Yao, Xinchao Hu, Ying Wang, Haihui Wang, Ration design of porous Mn-doped $Na_3V_2(PO_4)_3$ cathode for high rate and super stable sodium-ion batteries, Electrochimica Acta, 2019, 295, 262-269, doi: 10.1016/j.electacta.2018.10.150.

[56] Wenhao Yang, Wen He, Xudong Zhang, Guihua Yang, Jingyun Ma, Yaoyao Wang, and Chunlian Wang, $Na_3V_2(PO_4)_3$/N-doping hard carbon nanocomposites with sandwich framework derived from V-MOFs for cheap ultrahigh-rate and long-life sodium-ion batteries, ChemElectroChem, 2020, 6(7), 2020-2028, doi: 10.1002/celc.201801802.

[57] Hyeongwoo Kim, Hyojun Lim, Hyung-Seok Kim, Ki Jae Kim, Dongjin Byun, Wonchang Choi, Polydopamine-derived N-doped carbon-wrapped $Na_3V_2(PO_4)_3$ cathode with superior rate capability and cycling stability for sodium-ion batteries, Nano Research, 2019, 12, 397-404, doi: 10.1007/s12274-018-2229-z.

[58] Yanjun Chen, Youlong Xu, Xiaofei Sun, Baofeng Zhang, Shengnan He, Long Lia, Chao Wang, Preventing structural degradation from $Na_3V_2(PO_4)_3$ to $V_2(PO_4)_3$: F-doped $Na_3V_2(PO_4)_3$/C cathode composite with stable lifetime for sodium ion batteries, Journal of Power Sources, 2018, 378, 423-432, doi: 10.1016/j.jpowsour.2017.12.073.

[59] Xiaqing Chang, Qizhen Zhu, Ning Sun, Yibiao Guan, Ran Wang, Jiashun Zhao, Mingyu Feng, Bin Xu, Graphene-bound $Na_3V_2(PO_4)_3$ film electrode with excellent cycle and rate performance for Na-ion batteries, Electrochimica Acta, 2018, 269, 282-290, doi: 10.1016/j.electacta.2018.03.004.

[60] Qing Zhu, Hua Cheng, Xinmei Zhang, Liqing He, Lizhen Hu, Jianwen Yang, Quanqi Chen, Zhouguang Lu, Improvement in electrochemical performance of $Na_3V_2(PO_4)_3$/C cathode material for sodium-ion batteries by K-Ca co-doping, Electrochimica Acta, 2018, 281, 208-217, doi: 10.1016/j.electacta.2018.05.174.

[61] Wei Zheng, Ruichuan Gao, Tao Zhoua, Xiaobing Huang, Enhanced electrochemical performance of $Na_3V_2(PO_4)_3$ with Ni^{2+} doping by a spray drying-assisted process for sodium ion batteries, Solid State Ionics, 2018, 324, 183-190, doi: 10.1016/j.ssi.2018.07.006.

[62] Lina Zhao, Hailei Zhao, Zhaolin Li, and Zhihong Du, Superior High-Rate and Ultralong Lifespan $Na_3V_2(PO_4)_3$@C Cathode by Enhancing the Conductivity Both in Bulk and Surface, ACS Applied Material Interfaces, 2018, 10(42), 35963-35971, doi: 10.1021/acsami.8b12055.

[63] Qiong Zhenga, Hongming Yia, Wanqiu Liua, Xianfeng Lia, Huamin Zhang, Improving the electrochemical performance of $Na_3V_2(PO_4)_3$ cathode in sodium ion batteries through Ce/V substitution based on rational design and synthesis optimization, Electrochimica Acta, 2017, 238, 288-297, doi: 10.1016/j.electacta.2017.04.029.

[64] Atsushi Inoishi, Yuto Yoshioka, Liwei Zhao, Ayuko Kitajou, and Shigeto Okada, Improvement in the energy density of by $Na_3V_2(PO_4)_3$ Mg substitution, ChemElectroChem, 2017, 4(11), 2755-2759, doi: 10.1002/celc.201700540.

[65] Huaixin Liu, Yong Guo, Novel design and preparation of N-doped graphene decorated $Na_3V_2(PO_4)_3$/ C composite for sodium-ion batteries, Solid State Ionics, 2017, 307, 65-72, doi: 10.1016/j.ssi.2017.04.015.

[66] Bao Zhang, Hezhang Chen, Hui Tong, Xu Wang, Junchao Zheng, Wanjing Yu, Jiafeng Zhang, Jiangpeng Li, Wei Zhang, Synthesis and electrochemical performance of Ni doped $Na_3V_2(PO_4)_3$/C cathode materials for sodium ion batteries, Journal of Alloys and Compounds, 2017, 728, 976-983, doi: 10.1016/j.jallcom.2017.09.020.

[67] Huang Zhang, Ivana Hasa, Daniel Buchholz, Bingsheng Qin, Stefano Passerini, Effects of nitrogen doping on the structure and performance of carbon coated $Na_3V_2(PO_4)_3$ cathodes for sodium-ion batteries, Carbon, 2017, 124, 334-341, doi: 10.1016/j.carbon.2017.08.063.

[68] Huang Zhang, Ivana Hasa, Bingsheng Qin, Thomas Diemant, Daniel Buchholz, Juergen Behm, and Stefano Passerini, Excellent Cycling Stability and Superior Rate Capability of $Na_3V_2(PO_4)_3$ Cathodes Enabled by Nitrogen-doped Carbon Interpenetration for Sodium-ion Batteries, ChemElectroChem, 2017, 4(5), 1256-1263, doi; 10.1002/celc.201700053.

[69] Qing Qiu, Chao Li, Hui Liu, Yuxin Liao, Chong Zhao, Fushan Geng, Ming Shen, Jingxin Li, Wei Tong, and Bingwen Hu, NMR Evidence for the Multielectron Reaction Mechanism of $Na_3V_2(PO_4)_3$ Cathode and the Impact of Polyanion Site Substitution, The Journal of Physical Chemistry, 2021, 125(28), 15200-15209, doi: 10.1021/acs.jpcc.1c04099.

[70] G. Meligrana, S. Ferrari, L. Lucherini, J. Cele, F. Colo, J. Brugger, C. Richardi, R. Ruffo, C. Gerbaldi, European Chemical Societies, 2020, 7(7), 1652-1659, doi: 10.1002/celc.202000345**.**

[71] Dmitry Bokov, Abduladheem Turki Jalil, Supat Chupradit, Wanich Suksatan, Mohammad Javed Ansari, Iman H. Shewael,nGabdrakhman H. Valiev, and Ehsan Kianfar, Nanomaterial by Sol-Gel Method: Synthesis and Application, Advances in Material Science and Engineering, 2021, 5102014, DOI: 10.1155/2021/5102014.

[72] Dr. Jadhao Ujwala Ashokrao, Dr. Lagad C.E. and Dr. Ingole R. K., a review on application and importance of analytical methods for metallic preparations (incinerated ash) w.s.r. to XRF and XRD, World Journal of Pharmaceutical and Medical Research, 2023, 9(2), 47-54.

[73] E.S. Ameh, A review of basic crystallography and x-ray diffraction applications, The International Journal of Advanced Manufacturing Technology, 2019, 105, 3289-3302.

[74] http://prism.mit.edu>crystal_size_analysis

[75] xrd-principle-instrumentation-types-and.html

[76] James F. Rusling, Steven L. Suib, Characterizing Materials with Cyclic Voltammetry, Advanced Materials, 1994, 6(12), 922-930.

[77] Noemie Elgrishi, Kelley J. Rountree, Brian D. McCarthy, Eric S. Rountree, Thomas T. Eisenhart, Jillan L. Dempsey, A Practical Beginner's Guide to Cyclic Voltammetry, 2017, 95(2), 197-206.

[78] http://epgp.inflibnet.ac.in/epgpdata/uploads/epgp_content/S000014ER/P000272/M028089/ET/1520333353Paper2_Module29_e-text_Cyclicvoltammetry.pdf

[79] El Abadila Iffer, Mohammed Belaiche, Chouaib Ahmani Ferdi, Moustapha Elansary, Abdul Khader Sunar, Yanxia Wang, Yuliang Cao, International Journal of Energy Research, 2020, 45(2), 1703-1719. doi: 10.1002/er.5835.

[80] Guang He, Ashfia Huq, Wang Hay Kan, Arumugam Manthiram, β-$NaVOPO_4$ Obtained by a Low-temperature Synthesis Process: A New 3.3 V Cathode for Sodium-ion Batteries, Chemistry of Materials, 2016, 28(5), 1503-1512, doi: 10.1021/acs.chemmater.5b04992.

[81] Chih-Yao Chen, Kazuhiko Matsumoto, Toshiyuki Nohira, Rika Hagiwara, Improved Electrochemical Performance of $NaVOPO_4$ Positive Electrodes at Elevated temperature in an Ionic Liquid Electrolyte, Journal of the Electrochemical Society, 2015, 162(10), A2093-A2098.